MICHELE IMBRIALE

PhD THESIS

Inverse Heat Transfer Method for Ceramic Materials Thermo-Physical Properties Evaluation

Tutors

Chia.mo Prof. Cardone G.
Eng. Sottile D.

University of Naples Federico II & E.M.A. S.p.A.

2013

Contents

List of Figures

VI

List of Tables

Introduction

Investment casting, known as the lost wax process too, is one of the oldest and well-known manufacturing processes traced back to 5000 BC (Taylor 1983).

The investment casting process became to be used to produce components for the aerospace industry for its powerful characteristics and it has been particularly successful for the production of turbine blades and in particular for single crystal turbine blades.

As a rule the wax pattern, a disposable specimen in the shape and size of the final product, or the wax pattern assembly is invested into ceramic slurry followed by the application of a coating of dry refractory particles (*stucco*) which, when dried, gives a thin refractory shell.

The application of slurry and stucco is repeated, with drying between each successive coat, until the shell mould of sufficient thickness is achieved (Green-Spikesley 1979). Following completion of shell build, de-waxing and shell hardening processes get ready the shell for the following pouring of the molten metal into the expendable ceramic mould.

The production of the investment casting ceramic mould is a crucial part of the whole process (Mitchell 1999). The use of an expendable pattern confers an unique advantage to the investment casting process because the pattern is removed from the mould without any disturbance of the latter, but the continuous shell changing produces a random changing on the boundary conditions that directly affect the casting success.

A method to quickly find out the thermo-physical properties of the mould is desirable to reach two main goals:

- the *controlling* of the ceramic shell production;

- the *evaluation* of the ceramic thermo-physical properties in order to provide reliable boundary conditions to the *numerical simulation* and to well simulate the critical process of metal solidification;

The former may be obtained by means of the technique application on ceramic samples in a fixed time sequence, the latter by means of the technique application on a statistically relevant number of ceramic samples.

The importance of the numerical simulation of the casting process was getting increase in the last years because it may be one of the most important *cost-saving* method. In order to make sure the reliability of a numerical simulation the good correspondence between physical

model and mathematical model is required. The thermo-physical properties of the ceramic mould strongly influences the boundary condition imposed to the metal during solidification and it is because the technique proposed in this work may be helpful to increase the reliability of the numerical casting simulation because it is often based on fixed data that do not take into account the random variability of the mould building process and also the influence of the process parameters (i.e. hardening time, slurry and stucco composition, slurry viscosity) on the thermo-physical properties are partially or completely unknown.

The transient cooling process of a ceramic isotropic thin slab starting from high temperature down to room temperature will be experimentally investigated using IR thermography and the superficial temperature T_m will be compared against the surface temperature drop T_n numerically generated; Varying thermo-physical properties of the numerical model is possible to find out its value in correspondence on the minimum of the norm of the vectorial difference $\delta = (T_n - T_m)$; the technique modelling must be build to take into account the properties dependence on the temperature since the range of temperature must be necessarily wide.
This is a typical *inverse problem* (Kirsch 1996): given the effects (time variation of surface temperatures and heat fluxes) the causes (the material properties) must be estimated. Inverse problems are typical ill-posed problems since the solution can be extremely sensible to the noise and can be unstable;

The well-known *trust-region-reflective algorithm* (Coleman & Li 1994) will be used for the error minimization between experimental surface temperature and numerical surface temperature which is a parametric function depending on the unknown parameters. Also the error analysis will be carrier out.

Chapter 1

Investment Casting and Ceramic Materials

1.1   Investment Casting

The *investment casting* is an industrial process that involves the metallic production by means of an expendable pattern. The first process that is comparable to the present-day investment casting is one of the oldest, if not the oldest, metal shaping processes known to man. Since the Bronze Age to the Medieval times (in Europe) the investment casting technique was widely employed to make the most common metallic objects. In spite of the earliest origin the investment casting just became a successful industrial technique in the early 1940's in the USA and shortly after in the UK and was a combination of both the jewellers' and the dentists' skills, providing a route for the manufacture of relatively complex components of

precise shape and size, with good surface finish and in alloys which were difficult to work by other means.

When the technique began to be employed for aircraft parts manufacturing the process has seen a rapid and maintained expansion and development and now serves a wide range of applications, in both general and specialised engineering (Green-Spikesley 1979).
The use of the expendable patterns gives a formidable advantage to the process: the pattern is removed from the mould without any disturbance of the former and the dimensionally accurate components production is cheaper alternative than forging or machining since waste material is kept to a minimum. Of course the mould must have high thermal shock resistance to prevent cracking during metal pouring, chemical stability and have low reactivity with the metals being cast to improve the surface finish. Besides it must have sufficient mould permeability, thermal conductivity, and low thermal expansion to maintain an adequate thermal transfer through the mould wall to allow the metal to cool. Finally, the mould must be easily collapsible after casting to facilitate the knocking out and the cleaning operation (Sidhu et al. 2008). All these characteristics may be find out in the *ceramic material*. Before to give more information about the ceramic materials, will be explained the basic steps of the investment casting (fig. 1.1):

- *Wax Pattern Moulding and Assembling*;

- *Dipping in ceramic slurry system*;

- *Sprinkling of ceramic powder - stucco*;

- *De-waxing*;

- *Shell Hardening - Firing*;

- *Casting*;

- *Shell Removing and Cut-Off*;

- *Finishing*;

The *wax pattern moulding and assembling* is the first step and it is the modelling of the wax pattern to give it the exact edge and dimension (at least very similar) of the final metallic part. It's important to take into account that all wax parts will be metallic part and moreover the assembling may influence the liquid metal flow and the solidification process. So the assembling step is not only a linking of more wax patterns together, but an actual cast design step.

The production of the investment casting ceramic shell mould is performed with the repeating of the wax patterns *Dipping* in a slurry system and the *Sprinkling* steps as many time as shell thickness needs to reach the desirable value. At this step the shell appears like as a layer material. This process is a crucial part of the whole casting process. A single stuccoed slurry layer may take between 3-8 hours to dry. It's because the shell production is considered the most time consuming process of the whole investment casting process.

After all layers deposing and shell drying the wax pattern
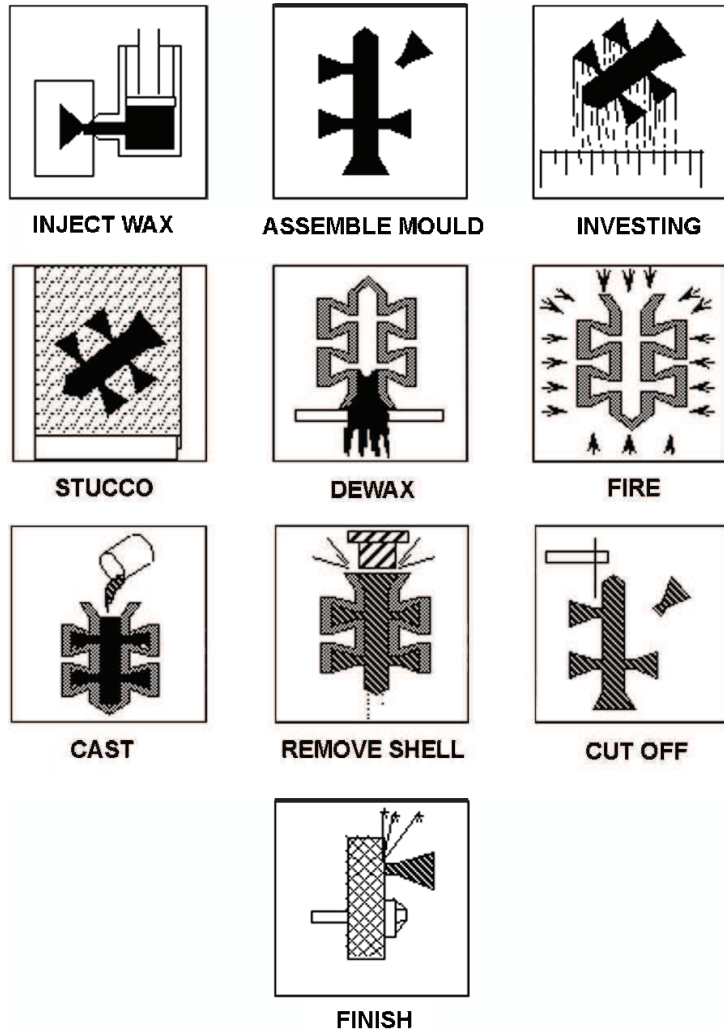
Figure 1.1: Sketch of the investment casting process (Jones et al. 2002) .

must be removed generally by means of a pressurized autoclave (in which steam provide the sufficient energy to melt the wax) even if others methods are tested (microwave heating or burning).

At this step the shell mechanical strength is not yet sufficient to withstand casting. Hence a firing process is generally performed to sinter the structure of the ceramic. Also this process is useful to remove residual pattern material and solvents remaining in the ceramic after de-waxing and to present the mould for casting at a predetermined and consistent temperature.

The *casting* consists in the pouring of the melting metal in the shell mould and its solidification (controlled or uncontrolled depending on the request characteristic of the product).

Finally the shell removal is performed and the metal product is finished to reach the exact final shape in the last steps, *Cut-Off* and *Finishing*.

Before introducing the details of the new inverse heat transfer technique the author has found it useful to summarize the general characteristics of ceramic materials, that are the material on which the technique will be applied.

1.2 General Properties of Ceramic Materials

The general and most widely accepted definition of a ceramic is given by Kingery et al. (1976): *A ceramic is a*

nonmetallic, inorganic solid.
The definition contains two *non-definition*. It's because
the term "ceramic" is referred to a process rather than a
particular chemical, physical or thermal property. In fact
the traditional ceramic process involves shaping, drying,
and firing of a raw material.

It's because Carter & Norton (2007) defines a ceramic
material *as the art and science of making and using solid.*
In spite of the uncertain definitions the ceramic material
have some particular characteristics:

- *Brittleness*, due to the mixed ionic-covalent bonding
  that holds the constituent atoms together. At high
  temperatures (above the glass transition tempera-
  ture) glass no longer behaves in a brittle manner; it
  behaves as a viscous liquid;

- *Low Thermal and Electrical Conduction*, the valence
  electrons are tied up in bonds, and are not free as
  they are in metals;

- *Compressive strength*, ceramics are stronger in com-
  pression than in tension, whereas metals have com-
  parable tensile and compressive strengths;

- *Chemical insensitivity*, a large number of ceramics
  are stable in both harsh chemical and thermal envi-
  ronments;

Although it is always possible to find at least one ce-
ramic that shows atypical behaviour, the properties we

have mentioned here are in many cases different from those shown by metals and polymers.

Table 1.1: Properties and applications of ceramics. Data from Carter & Norton (2007).

Property	Example	Application
Electrical	$Bi_2Ru_2O_7$	Conductive component in thick-film resistors Doped
	ZrO_2	Electrolyte in solid-oxide fuel cells
	Indium tin oxide (ITO)	Transparent electrode
	SiC	Furnace elements for resistive heating
	$YBaCuO_7$	Superconducting quantum interference devices
	SnO_2	Electrodes for electric glass melting furnaces
Dielectric	$\alpha - Al_2O_3$	Spark plug insulator
	$PbZr_{0.5}Ti_{0.5}O_3$ (PZT)	Micropumps
	SiO_2	Furnace bricks
	$(Ba, Sr)TiO_3$	Dynamic random access memories (DRAMs)

(Continued on the next page)

11

(Continued from previous page)

	Lead magnesium niobate (PMN)	Chip capacitors
Magnetic	$\gamma - Fe_2O_3$	Recording tapes
	$Mn_{0.4}Zn_{0.6}Fe_2O_4$	Transformer cores in touch tone telephones
	$BaFe_{12}O19$	Permanent magnets in loudspeakers
	$Y_{2.66}Gd_{0.34}Fe_{4.22}Al_{0.68}Mn_{0.09}O_{12}$	Radar phase shifters
Optical Doped	SiO_2	Optical fibers
	$\alpha - Al_2O_3$	Transparent envelopes in street lamps
	Doped $ZrSiO_4$	Ceramic colors
	Doped $(Zn, Cd)S$	Fluorescent screens for electron microscopes
	$Pb1 - xLa_x (Zr_zTi_{1-z})_{1-x}/4O_3$	Thin-film optical switches
	Nd doped $Y_3Al_5O_{12}$	Solid-state lasers
Mechanical	TiN	Wear-resistant coatings
	SiC	Abrasives for polishing Diamond Cutting tools
	Si_3N_4	Engine components

(Continued from previous page)

	Al_2O_3	Hip implants
Thermal	SiO_2	Space shuttle insulation tiles
	Al_2O_3 and AlN	Packages for integrated circuits
	Lithium-aluminosilicate glass ceramics	Supports for telescope mirrors
	Pyrex glass	Laboratory glassware and cookware

1.3   Ceramic Materials for Investment Casting. Shelling Process
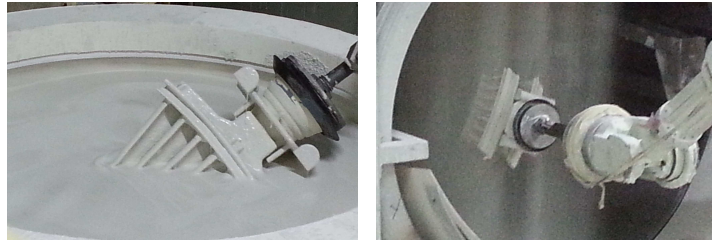
Figure 1.2: Dipping of the wax pattern in a ceramic slurry (left) and *"stuccoing"* with ceramic particles (right).

The production of the ceramic mould is a crucial part of the whole investment casting process (Mitchell 1999). Hence the checking and measuring of the shell properties may be a very important activity in order to prevent any defects that occur in metal products during casting.
The *a priori* estimation of the shell properties is very difficult because a lot of different materials are mixed together to give any particular characteristic to the mould. In example the first layer, which is applied directly to the wax pattern, is responsible for the re-producing of the surface finish and detail of the pattern or, in the solidification process, is responsible of the nucleation of crystals. Instead the backup layers build the shell strength, which support the metal.
After layers deposition and drying the ceramic mould mainly

must withstand the de-waxing process. Since most shell cracking and failure happen during the wax removal, the so-called *green (unfired) strength* takes great importance. Generally the green strength does not satisfy the required strength to withstand at the casting and it is because it is needful the *firing* step during which the sintering is totally or partially made. In the latter case a percentage of the original pores formed during the alternate deposition of slurry and stucco are preserved to ensure the shell permeability to the gases.
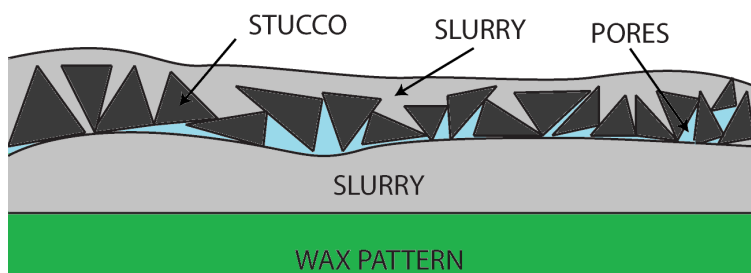
Figure 1.3: Sketch of slurry and stucco deposition with pores creation.

For the sake of completeness the main shell desirable characteristics are resumed in the following list (Yuan & Jones 2003):

- Green (unfired) strength to withstand wax removal without failure;

- Fired strength to withstand the weight of cast metal, but not so high to avoid residual stresses in the prod-

ucts (the shell must crack in a particular moment depending on the specific product);

- Thermal shock resistance to prevent cracking during metal pouring;

- Creep resistance to prevent dimensional changes within the mould wall and ultimately the casting;

- Chemical stability to prevent the mould-metal interaction;

- Mould permeability to allow trapped air permeate through the mould walls during metal pouring (achieved by means of porous ceramics);

- Thermo-physical properties (i.e. sufficient thermal diffusivity or conductivity) such as to maintain an adequate thermal transfer through the mould wall and hence allow the metal to cool; the shell is the *boundary condition* for the *metal system* during cooling and solidification and it can directly influence the quality of the products.

In many traditional applications, particularly in structural and electrical applications, the sintered ceramic component is required to have minimum porosity (Carter & Norton 2007). However, in any specific applications, such as investment casting, porosity is not just desirable, *it is required* in order to allow the gases leakage and so avoid any defects in the final products or avoid shells cracking

in a not desirable step of the cooling. Several different methods can be used to produce porous structures:

- Use particles with an irregular, angular shape and rough surface to obtain micro-porosity;

- *Underfire* a green compact to leave a large amount of fine pores;

- Add organic particles (diameter higher than $20\mu m$) to the powder mixture; when these burn out they will leave behind porosity;

- Use a binder system that contains a foaming agent and produces a large amount of gas bubbles in the mixture;

- Impregnate a foam that has a continuous porosity and then burn it out;

- Use a glass composition that phase separates and then leaches out (e.g., using an acid) one of the phases to produce porous glasses.

For the investment casting process the first two methods are usually employed.
Furthermore the shell mould is generally composed by different ceramic materials, hence the checking and the controlling of its properties are an important step both to ensure the required mould properties during casting and to provide a reliable data for casting simulation.

The interaction between the different materials to produce the thermal properties are difficulty estimable, hence *a posteriori* analysis may be the simplest and the most accurate way to take under control the shell behaviour, especially because the *de-waxing* and *Shell Hardening - Firing* steps may modify the ceramic properties by sintering (Randall 1996).

The present work deals with a fast method to check the thermo-physical properties of a ceramic sample in a wide range of temperature without perform a lot of successive steps and measurements. In fact to evaluate thermal diffusivity, thermal conductivity and the consequent volumetric specific heat is generally necessary to perform an equal number of measurements at a large number of temperature steps by means of different machineries (Parker et al. 1961, Taylor & Maglic 1984, Meola et al. 2002), by increasing the specific cost. In the present work will be present an innovative technique to evaluate both thermal diffusivity and conductivity by means a single procedure (inverse heat transfer) and a single instrument (IR-Camera). Moreover will be evaluate the properties dependence on the temperature.
It is important to point out that the porosity of the ceramics is closely linked to the shell thermo-physical properties. In fact a random distribution of porosity and its amount produces random thermal diffusivity and conductivity in the ceramic shell and a large number of experimental measurement may be necessary to take under control the thermal effect on the casting process. Hence the

development of a fast method for the evaluation of global thermal properties may be very useful in the investment casting process.

Of course the unification of more measurements into a single measurement may decrease the technique accuracy, but in the properties monitoring it is generally not required the highest accuracy, but a relative measurement for taking into account the *property changing* rather than the absolute value of the properties.

Chapter 2

IR Thermography

Infrared thermography is a non-contact temperature measurement technique: the measurement is performed by means of the infrared camera, which detects the electromagnetic energy radiated in the IR spectral band from an object and converts it into an electronic signal. The radiation energy emitted by a body mainly depends on the body surface temperature, but other parameters are involved in the phenomena. As a matter of fact the electromagnetic energy emitted by the body surface has to passes through both an interposed fluid, e.g., air, and a system of lenses and a filter and it finally reaches the thermal sensor which is responsible of the transduction into an electronic signal. When both surface emissivity of the body and the absorption of the crossed means are known, it's possible to associate the radiation energy to the temperature: the electrical signal - temperature correlation is generally known as the calibration correlation. The most

important characteristic of the IR Thermography is the
2-Dimensional temperature recording. For this reason in
the recent decades the IR thermography was firstly devel-
oped in the scientific research and then in the industrial
application. Nowadays the infrared systems are mostly
used in conjunction with personal computers both for the
visualization of the 2D measurements and for their quan-
titative analysis. The electronic signal produced by the
sensor is therefore elaborated by a dedicated hardware
which outputs the measurements results in the form of
computer files, containing general information about the
scanning conditions and the camera and the intensity of
radiation for each point of the two-dimensional radiation
map. These files are called IR images or thermograms,
and dedicated software can subsequently be used to visual-
ize them or for specific further elaboration. Modern ther-
mographs for qualitative measurements make wide use of
FPA sensors and the thermograms can be usually visu-
alized directly on the thermograph. The next paragraph
deals with the bases of the electromagnetic body radia-
tion and the radiative heat transfer in order to summarize
the physics phenomena that involves the IR thermography
measurements.

2.1   Black Body Radiation

*All objects in the physical universe which are not at ab-
solute zero radiate energy in the form of electromagnetic
waves. (Merritt & Hall 1959)*

The emission spectrum, which is the evolution of emitted energy as a function of wavelength, depends on temperature and on the characteristics of the bodies surfaces.

Results of observations on the nature of the spectral distribution of the radiation from a blackbody are shown in the follow figure.
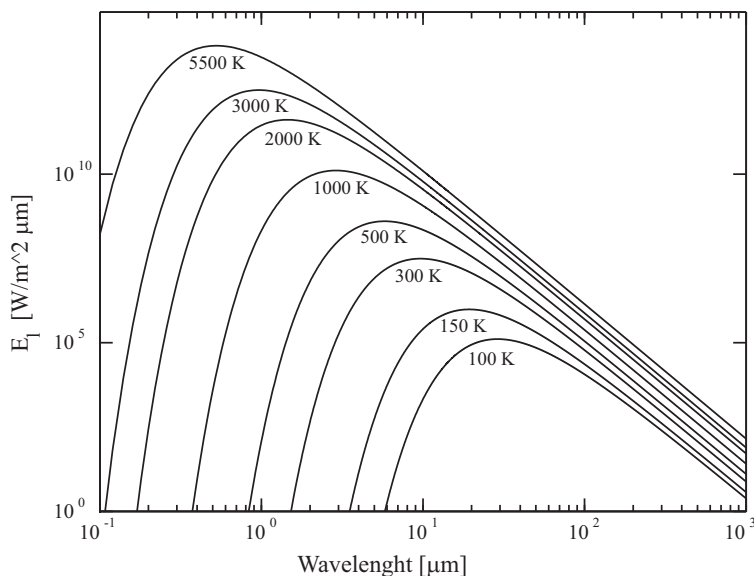
Figure 2.1: Plank's law: the wavelength-specific emitting power of a blackbody at temperatures indicated.

The laws which describe this emission spectrum make use of the concept of blackbody. The blackbody is a ideal body that emits and absorbs the maximum amount of radiation at any given wavelength and it represents a theoretical concept that sets an upper limit to the emission

of radiation at in accordance with the second law of thermodynamics. The energy emitted by a blackbody is given by Planck's law (drawn in Figure 2.1):

$$E_\lambda\left(T\right) = \frac{C_1}{\lambda^5 \left(e^{\frac{C_2}{\lambda T}} - 1\right)} \qquad (2.1)$$

where E_λ, measured in $Wm^{-2}\mu m^{-1}$, is the wavelength-specific emitting power of a blackbody at absolute temperature T at the wavelength λ , and and $C_1 = 2\pi\hbar c^2 = 3.74 \times 10^{-8} W\mu m^4 m^{-2}$ and $C_2 = \frac{\hbar c}{k_B} = 1.44 \times 10^4 \mu m K$ are the first and second radiation constants.
The total energy emitted by a blackbody is the integral of equation 2.1 over the entire wavelength spectrum and is expressed by Stefan-Boltzmann's law:

$$E\left(T\right) = \int_0^\infty E_\lambda\left(T\right) \, \mathrm{d}\lambda = \sigma T^4 \qquad (2.2)$$

where $\sigma = 5.76 \times 10^{-8} \frac{W}{m^2 K^4}$ is the Stefan-Boltzmann constant. Besides the the wavelength λ_{max}, that is the wavelength referred to the E_λ maximum, is linked to the absolute temperature through the Wien's displacement law:

$$\lambda_{max} T = 2898 \mu m K \qquad (2.3)$$

The equation 2.3 shows that bodies at temperatures equal to $300K$, $573K$ and $1273K$ have the maximum monochromatic emitted energy respectively at $9.9\mu m$, $5.1\mu m$ and $2.3\mu m$.
Real bodies generally emit only a fraction of the energy

emitted by a black-body at the same temperature (figure 1.2); this fraction is expressed by the monochromatic hemispherical emissivity ε_λ, which depends on the body material, on the surface roughness of the body, on its temperature, on the wavelength, on the direction of emission and so on. 2.1 and 2.2 therefore become:

$$E_\lambda\left(T\right) = \frac{\varepsilon_\lambda C_1}{\lambda^5\left(e^{\frac{C_2}{\lambda T}}-1\right)} \tag{2.4}$$

and

$$E\left(T\right) = \int_0^\infty \varepsilon_\lambda E_\lambda\left(T\right)\,\mathrm{d}\lambda \tag{2.5}$$

A body characterized by an ε_λ independent of the wavelength is called gray body. A gray body emits at every wavelength always the same fraction of the energy emitted by a blackbody. For a gray body:

$$E = \varepsilon\sigma T^4 \tag{2.6}$$

The emissivity is an important feature of all real bodies and it must to be known to perform any measurement of the emitted energy by the bodies: it is a fundamental characteristic for IR Thermography too. The IR Camera works in fixed wavelength in the IR-band and because the most of the real bodies can be considered grey bodies it's possible to know the monochromatic emissivity at any wavelengths or in any wavelength range to perform an accurate thermography. Unfortunately some materials, like ceramic material, don't have the monochromatic emissivity approximately constant with varying wavelength and

we need to know the monochromatic emissivity average
in the working IR-band of the IR-Camera to perform an
accurate temperature:

$$\bar{\varepsilon} = \frac{\displaystyle\int_{\lambda_1}^{\lambda_2} \varepsilon_\lambda E_\lambda \, \mathrm{d}\lambda}{\displaystyle\int_{\lambda_1}^{\lambda_2} E_\lambda \, \mathrm{d}\lambda} \tag{2.7}$$

It is also important to notice that ε_λ depends on the
angle of view θ and it decreases dramatically when θ be-
comes higher than about 60° (see figure 2.2).

The sensor of a thermograph is usually sensitive only
to a limited band of the infrared and the measurements
basically follow Planck's law. The infrared band has wave-
length comprised between 0.72 μm and 1'000 μm and is
usually subdivided in four zones:

- *Near IR*, with radiation wavelength comprised be-
  tween 0.75 μm and 3 μm;

- *Intermediate IR*, with radiation wavelength comprised
  between 3 μm and 6 μm;

- *Far IR*, with radiation wavelength comprised be-
  tween 6 μm and 15 μm;

- *Extreme IR*, with radiation wavelength comprised
  between 15 μm and 1000 μm.
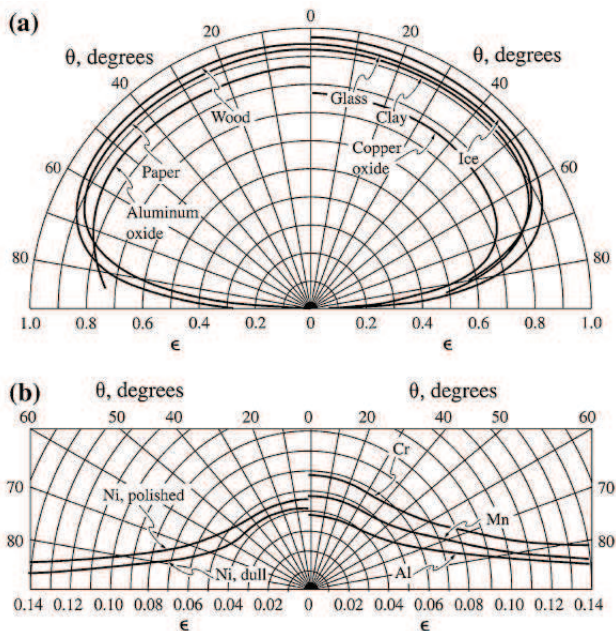
Figure 2.2: Directional emissivity: *(a)* for several non-metals; *(b)* for several metals (Modest 2003, Schmidt & Eckert 1935).
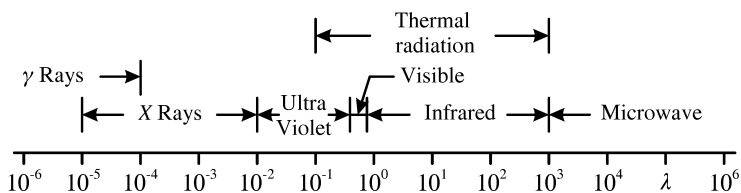
Figure 2.3: Electromagnetic spectrum and thermal radiation portion of the electromagnetic spectrum. Wavelength λ is reported in μm. From Astarita & Carlomagno (2013).

2.2   IR Detectors and their Characteristics

The purpose of the infrared detector is to transform the electromagnetic radiation they absorb in an electric signal. There are two main families of sensors: thermal detectors and photon detectors. *Thermal detectors* used to be the most widespread and they are based on the variation of electrical resistance of a film of semiconductor when it is hit by an incident radiation. The main characteristic of this family of detectors are a flat output signal, which can be considered practically constant in a large band of wavelengths, and response time relatively long when compared to photon detectors. The signal P emitted by a thermal detector may be considered proportional to the input radiative power:

$$P\left(T\right) = \int_{\lambda_1}^{\lambda_2} \varepsilon_\lambda\left(T, \theta\right) E_\lambda\left(T\right) R\left(\lambda\right) \mathrm{d}\lambda \qquad (2.8)$$

where $R\left(\lambda\right)$ is the response of the instrument, θ is the angle of view between sensor and radiating surface and $[\lambda_1, \lambda_2]$ the sensitivity band of the instrument. In the hypothesis of gray body, equation 2.8 becomes:

$$P\left(T\right) = \varepsilon\left(\theta\right) \int_{\lambda_1}^{\lambda_2} E_\lambda\left(T\right) R\left(\lambda\right) \mathrm{d}\lambda = \varepsilon\left(\theta\right) P_o\left(T\right) \quad (2.9)$$

where $P_o\left(T\right)$ is the signal obtained by a black-body at the same temperature. *Photon detectors* are instead characterized by semiconductors which emit a number of

electrons directly proportional to incident radiating energy. The incident photons are captured by the detector and converted into a variation of electrical potential in the case of photoconductive detectors, and in a variation of electrical resistance in the case of photovoltaic detectors. The energy of the photons is inversely proportional to their associated wavelength and the disappearance of photoelectric activity at wavelengths higher than the "cut-off" wavelength λ_c indicates that in this case the energy associated with photons is not sufficient to generate the emission of electrons. Photons must therefore have an energy higher than the so called forbidden energy gap E_g characteristic of each semiconductor. The cut-off frequency is given by:

$$\lambda_c = \frac{\hbar c}{E_g} \tag{2.10}$$

where E_g is expressed in *Joule*.
In general E_g is low at ambient temperature and increases as temperature decreases. This is the reason why these sensor need to be cooled and must operate at very low temperature (usually of the order of $75K$). The energy associated to a single photon at a given wavelength is $Q = \frac{\hbar c}{\lambda}$, so the total number of emitted photons is obtained dividing equation 2.1 by Q to obtain the number N_{λ_o} of emitted photons at a single wavelength and integrating over the whole spectrum to obtain:

$$N_o = \int_0^\infty N_{\lambda_o} \, \mathrm{d}\lambda = \frac{0.37}{k}\sigma T^3 \tag{2.11}$$

which has dimensions of $photons \cdot cm^2 \cdot s^{-2}$ and express the dependence of blackbody total emission from the cube of temperature. Almost all infrared detectors are sensitive only in a limited wavelength band; the integral in equation 2.11 needs therefore to be calculated not in $[0, \infty]$ but in $[\lambda_1, \lambda_2]$ which is of course the sensitivity band of the sensor. Thermographs work in the majority of the cases in air and, as a consequence, the sensitivity bands used for infrared sensors are those in which the transmittance of air is the highest. From this point of view, two main bands are recognized: the short wave window and the long wave window (see figure 2.4).
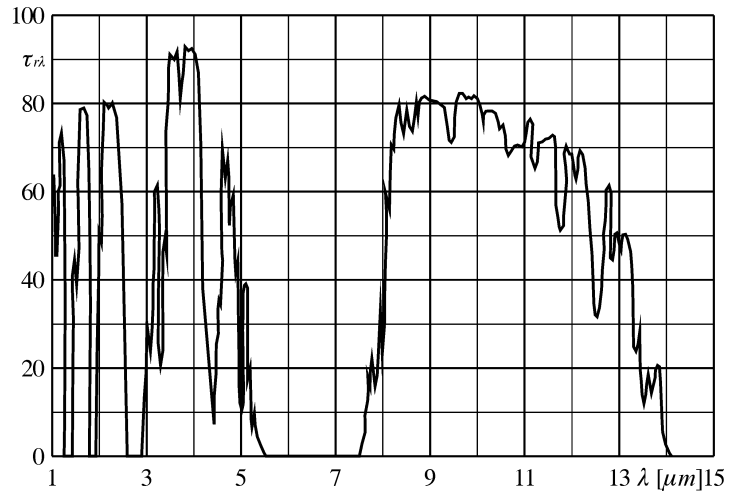
Figure 2.4: Spectral transmittance of a 1 km thick atmospheric layer in the near, middle and long infrared bands as a function of λ. Data from Astarita & Carlomagno (2013), Gebbie et al. (1951).

Several materials are used in the realization of IR detectors. The most widely used in the short wave window are Indium Antimonide ($InSb$) and Platinum Silicide ($PtSi$), while in the long wave window Mercury-Cadmium-Tellurite (MCT or $HgCdTe$) and Gallium Arsenide ($GaAs$) are worth mentioning. Fig. 2.5 reports shows the spectral response for these and other detectors.
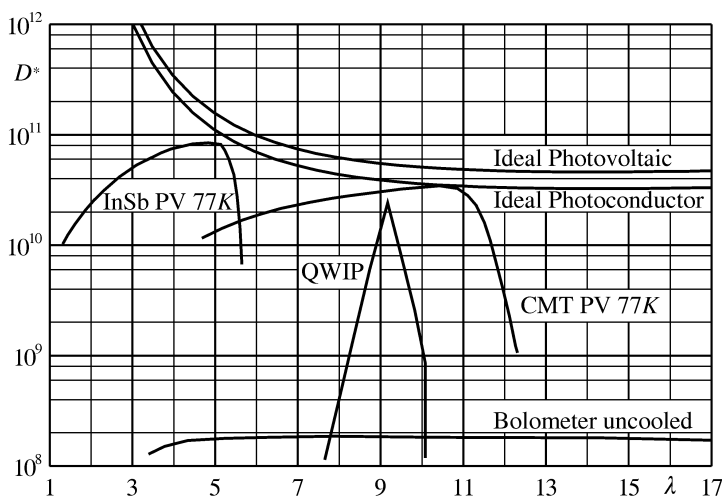
Figure 2.5: Spectral response for various detectors. Wavelength λ is reported in μm.

The choice of operative wavelength, hence of the thermograph with the appropriate sensor, depends on several factors, the most important of which is related with the transmittance of the fluid in which the surface under exam is immersed. In air longer wavelengths are preferred when the distance between sensor and body is high, be-

cause the presence of water vapour can create problems in the short-wave window. Other considerations regard the surface emissivity coefficient, which for some materials is higher at shorter wavelengths or *vice-versa*.

2.3   Scanning Methods

The main and more interesting characteristic of a thermographs is the capability to perform full two-dimensional measurements of the surfaces under exam. In order to investigate the whole field mainly two different systems are used: mechanic scanning and electronic scanning. The former is employed in the older cameras in which a single sensitive element is employed and an opto-mechanical system is needed to let radiation emitted by different points of the surface hit the sensor and the field of view is scanned in different ways, along the horizontal or vertical directions. Instead modern cameras make use of the so called Focal Plane Array (FPA), in which thousands of detectors are situated on a square array; with this arrangement each detector measures radiation from a portion of the field of view and no additional device is needed to measure the whole field of view.

Opto-Mechanical Systems

The scanning system is usually located between the lens and the detector, and it is used to define the viewing direction of the thermograph. The system makes use of a

complicated system which involves a rotating prism, an oscillating mirror and several other fixed mirrors. When high frequency of acquisition are needed the rotational speed of the prism can reach high velocities. Although of older concept, these systems can be extremely accurate and are still sometimes preferred when the limitations of the FPA systems, described in the next paragraph, are considered unacceptable.

Focal Plane Array

The two-dimensional sensor Focal Plane Array (FPA) is used by most recent thermographic cameras. It is constituted by a square or rectangle substrate on which an elevated number of detectors are integrated. The most common detectors in use in FPA sensors are:

- *Platinum Silicide* (PtSi): it operates in the first atmospheric window from 2 μm to 5 μm; it is characterized by a great degree of simplicity hence low costs. It has a good thermal resolution (of the order of the tenth of degree) but it's unstable and needs calibration every time the thermograph is switched on; furthermore it requires a cryogenic cooling through a Stirling cycle;

- *Indium Antimonide* (InSb): it operates in the 2-5.6 μm window, it is characterized by great sensitivity, it is very stable and doesn't need frequent calibration, and it has a very good thermal resolution (about $0.025K$) and a reasonable scanning fre-

quency. It is cooled by a closed Stirling cycle. For its characteristics it is much more expensive than the PtSi sensor;

- *Gallium Arsenide Quantum Well Infrared Photodetector* (GaAs QWIP): it operates at long wavelength, 8-9 μm . It is characterized by even greater performance than the InSb both in thermal resolution and in scanning frequency.

- *Non-cooled two-dimensional sensor* (microbolometric): it operates at long wavelength,$7.5-13\mu m$. The microbolometric IR camera has lower performance than the InSb both in thermal resolution and in scanning frequency, but its ductile characteristics meet the industrial needs.

The presence of an elevated number of detectors represents a fundamental change with respect to the classical thermographic systems, because the image viewed by the thermograph focuses on the FPA and is subdivided among all its detectors. This design allows FPA IR systems to avoid the need of mechanical scanning system, as the rotating polygons or galvanometric mirrors, which are used in classic IR system where a single detector scans the whole surface viewed by the thermograph. One consequence of this is that FPA sensors can have an integration time from $\frac{1}{30}$ to $\frac{1}{60}$ of second, which is much longer than the nanoseconds usually associated with classic IR systems; thanks to longer integration times, FPA based thermograph can have higher sensitivity and low

electronic noise. An FPA sensor is made by thousands of sensitive elements, and each one of them can have a slightly different reaction when hit by the same infrared radiation; this can result in non uniform images even when viewing surfaces at constant temperature. This problem is present in all FPA cameras, and is solved by appropriately regulating the gain of each pixel; this process of internal calibration is performed every time the camera is switched on, but it can also be forced via control software. Another problem related with this kind of cameras is the unavoidable presence of dead or defective pixels. When a dead pixel is detected the thermograph automatically substitutes their measurements with interpolated values from nearby pixels. The percentage of dead pixels can range from less than 1% to about 2% for less expensive devices. The FPA sensor is becoming the market standard thanks to its good spatial resolution and to the elimination of the costly and more fragile opto-mechanical scanning systems needed by classic IR systems.

2.4 Distinguishing Characteristics of Thermographs

The quantitative performance of a thermograph depends on some fundamental parameters which define its characteristics: thermal sensitivity, frequency of acquisition, spatial resolution and signal intensity resolution:

- The sensitivity of a thermograph is expressed by the

NETD (Noise Equivalent Temperature Difference,
which is the difference in temperature between two
images generating a signal equal to the background
noise: when the difference in temperature between
two images is lower than the NETD the thermo-
graph wont sense that difference. The NETD is
evaluated at a known temperature of the sample,
and can vary from $0.07K$ to $0.5K$ for measurements
at ambient temperature;

- The frequency of acquisition represents the speed
  at which images are recorded by the thermograph.
  The whole field of view is investigated by horizontal
  or vertical scanning systems in a given number of
  lines or columns; a frequency of acquisition per line
  can therefore be defined and some thermograph, in
  order to increase their frequency of acquisition, can
  record a limited number of lines rather than their
  full field of view.

- The spatial resolution is the capacity of the system
  to distinguish elements of the surface of small di-
  mension and to correctly measure their temperature.
  For a given frequency of acquisition the spatial reso-
  lution of the images is in general determined by the
  dimension of the sensor. In general the spatial reso-
  lution is defined by the Instantaneous Field Of View
  (IFOV) of the sensor or, better yet, by the number
  of IFOV which are comprised in the total field of
  view. In theory, the IFOV is the ratio between the
  dimension of the sensor and the focal length of the

lens, but this is only an idealized geometrical defini-
tion; in practice the quantity of interest is the small-
est size distinguishable by the thermograph. The
evaluation of the spatial resolution is fundamental
for experimental applications, when it is not always
possible to locate the thermograph close to the mea-
sured surface. In such cases it is also important to
check if the chosen thermograph has the possibility
to mount telephoto lenses;

- The intensity resolution is usually described in terms
of the number of gray level used to digitalize the
thermal image, and it therefore also defines the mini-
mum temperature difference which is digitalized with
two different gray levels. For example, a 12 bit
thermograph digitalizes the image in $2^{12} = 4'096$
gray levels; if the temperature interval measured
by the thermograph is, say, $-30^{o}C$ to $150^{o}C$ then
its intensity resolution in terms of temperature is
$\frac{180}{4'096} = 0.044^{o}C$. Usually thermograph include the
possibility to change the measurable temperature in-
terval with the use of proper filters.

2.5 InfraRed-Camera Fundamen-
tal Relationship

The energy detected by a IR-camera exclusively depends
on the body surface temperature if:

- the body is a blackbody;

- no matter is interposed between body and IR-Camera;

In these hypothesis the body temperature T can be easily linked to the total radiation I (also called *Isotherm Unit*) detected by the camera by means of the follow equation:

$$I = \frac{R}{\left(e^{\frac{B}{T}} - F\right)} \qquad (2.12)$$

where R, B and F are the three calibration constants which depend on the characteristic of the thermograph. Because the thermograph is sensitive in a limited range of wavelength (much narrower than whole thermal radiation range) the equation 2.12 is much more similar to the *Planck's law* (eq.2.1) rather than Stefan-Boltzmann's law(2.2). The last equation is easily invertible to obtain the temperature dependence on the Isotherm Unit I:

$$T = \frac{B}{\left(\ln F - \frac{R}{I}\right)} \qquad (2.13)$$

If the IR-detection is performed on a real body with any matter interposed the energy captured by camera become:

$$I = \tau \varepsilon I_b + \tau \rho I_{env} + (1 - \tau) I_{atm} \qquad (2.14)$$

where τ is the transmittance coefficient of the interposed matter, ε is the body emittance and ρ is the body reflectance. As a consequence of the Kirchoff's law $\rho = 1 - \varepsilon$ the equation becomes:

$$I = \tau \varepsilon I_b + \tau (1 - \varepsilon) I_{env} + (1 - \tau) I_{atm} \qquad (2.15)$$
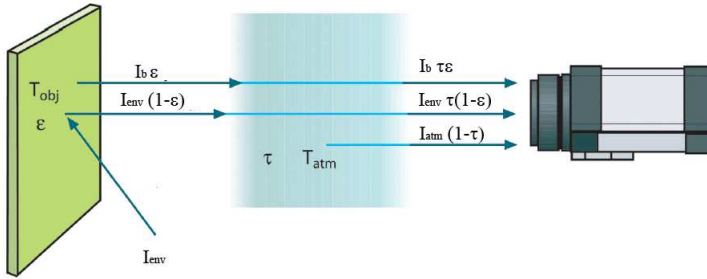
Figure 2.6: Schematic rapresentation of the eq 2.15.

The values of I_b, I_{env} and I_{atm} are corresponded, respectively, to the temperatures of the body, of the environment and of the atmosphere. The fundamental relationship points out the most important external variables influencing the quality of the measurement:

- the emissivity, that generally depends on the body's material, surface finish, angle of view and surface temperature;

- the transmittance of the interposed matter. Between the thermograph and the body and the possible presence of other transparent or reflective bodies present in the optical path;

In reference to the eq. 2.15, the second and third terms of the right hand side are two disturbance terms in the temperature measurement and, as a consequence,ε must be

as high as possible (ρ as low as possible) and environment temperature must be relatively different in reference to the object temperature. The matter interposed between camera and body, usually atmosphere, also influences the measurement through its absorption coefficient. If this coefficient is high, the fluid absorbs a significant percentage of the radiations emitted by the body and only the not-absorbed fraction of the radiation can reach the camera (the phenomena is token into account in the trasmittance coefficient).

2.6   InfraRed-Camera Calibration

The calibration constants relative to the whole measurement field of the thermograph are given by the manufacturer; in this case they can only take into account the characteristic of the thermograph, and not all other parameters just mentioned. As a consequence, when the thermograph is used for precise quantitative measurements it is preferred to measure these constants in situ through a calibration process done in test conditions. When thermographic measurements are made, it is important to minimize all causes which can have negative effects on the precision of the measurements. The elaboration of the digital output of the thermograph should be done taking into account that:

- The relationship between temperature and the intensity of radiation reaching the sensor is not linear;

- The electromagnetic signal can be altered by the presence of bodies, such as wind tunnel windows, in the optical path;

- The external environment can source of direct or reflected emissions and can therefore influence the radiation absorbed by the sensor;

The calibration constants are obtained using a blackbody and the procedure consists in:

- Having the thermograph look at the black body replicating the optical path that will be used in experiments;

- Recording simultaneously the black body temperature (with the help of a precision thermometer inserted in the thermostatic bath) and the *Isotherm Units* measured by the thermograph;

- Fitting of the experimental points by the equation 2.13 through a regression process in which the constant R, B and F are estimated.

2.7   Thermograph FLIR S65

In this work the FLIR S65 IR-camera has been used (see Figure 2.7). Of course a PC system is used to control the camera and record the time depending sequences of IR images.

Figure 2.7: IR-camera FLIR S65.

The FLIR S65 is fitted out with a non-cooled two-dimensional sensor (microbolometric) and it is used in the E.M.A. S.p.A. for a wide variety of applications. Its characteristics are listed in the Table 2.1.

2.7.1 FLIR S65 Noise Evaluation

In order to evaluate the IR-Camera noise variance at high temperature an experimental acquisition has been performed using an high temperature source fixing the temperature in correspondence with a fixed step. The high temperature source is the ELITE TMH16/50/160 (shown in the Figure 2.8) and the technical characteristics are summirized in the Table 2.2.

Because the inverse method needs to work over a wide

Property	Value
Detector type	Microbolometer not cooled
Spectral range	$7.5 - 13\ \mu m$
Field of view	6.64^{o}
IFOV	$0.36mm$ @ $1.0m$
Acquisition Frequency	$50Hz$
Temperature Range	Five Selectable Range up to $2000^{o}C$
Accuracy	$\pm 2^{o}C$ or 2% of Measured Temperature

Table 2.1: FLIR S65 - Technical characteristics.

range of temperature, the noise variance estimation has been performed at high temperature and hence the standard deviation has been found out. The camera noise is a fundamental information for error analysis and it is because it is so important to evaluate it. The Figure 2.9 shows one frame of the black body at $792^{o}C$ and the Figure 2.10 shows the temperature noise distribution over 10'000 consecutive frames in the same pixel in correspondence with the central point (marked in the figure).

The results show that the IR-camera at high temperature (close to the high temperature imposed in the experimental run 4) produce a noise with mean equal to zero and standard deviation equal to $\sigma = 0.55K$. In order to numerically evaluate the noise influence on the methodol-

Figure 2.8: High temperature source ELITE TMH16.

ogy reliable this data has been used in par. 3.2.4.

Property	Value
Maximum temperature	1500^oC
Heating rate	1.5 hours to 1400^oC
Stability	$< 0.5^oC$
Emissivity	0.998
Control thermocouple	Type R

Table 2.2: High temperature source. Technical characteristics.
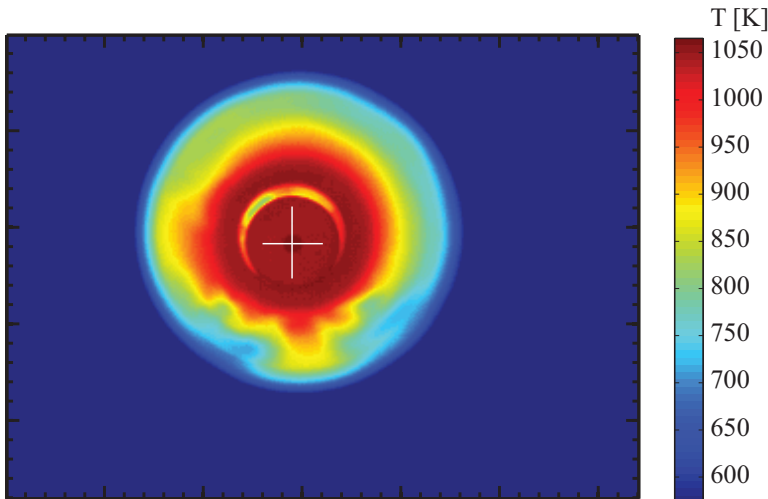
Figure 2.9: Thermogram of a the black body as seen by the S65 thermograph. The temperature at stationary conditions is 792^oC, or equivalently $1065K$.
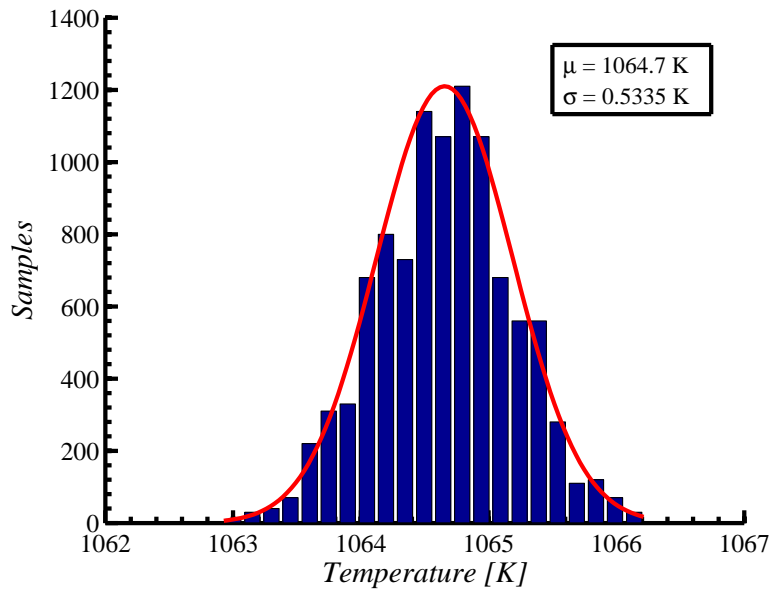
Figure 2.10: Temperature distribution for the thermograph
S65 at $1064.7K$ over 10'000 samples in reference on the marked
point in Figure 2.9. The red line ia a Gaussian curve with the
same standard deviation.

Chapter 3

Inverse Problems

An inverse problem (Vogel 2002) typically is the estimation of certain quantities based on indirect measurements of these quantities. This class of methods are widely employed both in scientific and industrial applications (Banks & Kunisch 1989, Bertero & Bioccacci 1998, Kirsch 1996, Natterer 1986) and the field of applicability ranges from biomedical to geophysics science.

The heat transfer is one of the most important application field for inverse methods.

Unfortunately in case of inverse heat transfer the procedure of the unknown parameter estimation is often not *well-posed* (Tikhonov 1977, Tikhonov et al. 1998). The conditions for a problem to be considered a well-posed problem are (Hadamard 1923):

- the solution to the problem must be exist;

- the solution must be unique;

- the solution must be stable (i.e., small changes of problem parameters cause only small changes in solution and vice-versa);

An inverse problem often doesn't keep the third rule and it means that noise in the data may give rise to significant errors in the parameter estimation. Mathematical techniques known as *regularization methods* (Engl et al. 1996, Morozov 1993) have been developed to deal with ill-posedness.

3.1   Inverse Methods for Heat Transfer

The inverse method applications on the heat transfer (IMHT) science may be divided in two main group:

- heat flux sensors;

- inverse method for material properties;

in both cases by measuring of the effect (the surface temperature evolution) will be possible to find out the causes. The causes are the discriminant factor between the groups: the heat transfer between a body and ambient depends on the boundary conditions (*convective coefficient, emissivity*) and the body's materials characteristic (*thermal diffusivity, thermal conductivity*). If the causes to be found out are the boundary conditions the inverse method is called *heat flux sensor*, while if the causes are the body's

characteristic the method may be classified as an *inverse method for material properties.*

The aim of this work is the developing of a method to quickly find out the thermo-physical properties of the ceramic material employed in the investment casting and in particular *thermal diffusivity* and *thermal conductivity.* The fundamental idea is to develop an inverse method for material properties (second group) in which the transient cooling process of a ceramic isotropic thin slab starting from high temperature down to room temperature is experimentally investigated using IR thermography and the surface temperature T_m is compared against the surface temperature drop T_n numerically generated; Varying thermo-physical properties on which temperature T_n depends, it is possible to find out the properties in correspondence with the minimum norm of the vectorial difference $\delta = (T_n - T_e)$. Since the range of temperature must be necessarily wide the technique modelling is built to take into account the properties dependence on the temperature.

Because the inverse methods are always ill-posed, the calculation technique must some particular dodge to minimize the disturbance. In the past a further complications and source of instability was the temperature sensors layout: in fact the sensor was inside the model and not on its surface. The use of thin film surface resistance thermometers first and of infrared thermography have later permitted to overcome this kind of problem.

The need to develop a new METP comes from any physical considerations. Since the physical models are the same in both cases and because the heat flux sensors are certainly the widely studied methods (Astarita & Carlomagno 2013), it seems needful to itemize the main heat flux sensors. Furthermore it must be pointed out that any heat flux sensors may be applied like as inverse method for material properties.

- *Heated thin foil* sensor: the slab usually consists of a thermally thin metallic sheet (foil), or a printed circuit board, steadily and uniformly (in space) heated by the Joule effect. Strictly speaking, the foil may be heated also in a different way (e.g. by a radiation heat flux impinging on the foil) but then, the heat flux distribution over it should be precisely known. The convective heat transfer coefficient can be computed by measuring the heat input as well as the foil surface temperature with the infrared scanner and by performing a complete energy balance. Because of the thermal thinness of the foil, the temperature can be measured on either of the slab surfaces. However, it is possible to apply this sensor also to nonthermally thin foils; the *heated thin foil technique* does not take into account any material properties and it is because it can not be applied as a inverse method for material properties evaluation;

- *Thin film* sensor: a thermally thick slab is used as a sensor and the convective heat transfer coefficient

is inferred from the theory of unsteady heat conduction in a semi-infinite solid. The name of the sensor classically derives from the resistance thermometer (often a very thin platinum film), which is bonded to the slab surface. Clearly, the thin film itself must have negligible heat capacity and thermal resistance as compared to the slab layer affected by the exchanged heat flux. When this sensor is used in combination with an IR scanner, the thin resistance thermometer does not exist but the slab surface in contact with the exchanging fluid must be necessarily viewed by the scanner.

- *Thin skin or wall calorimeter* sensor: the sensor is made of a thermally thin slab (skin) which is used as a perfect calorimeter. Being that the slab is thermally thin, the temperature can be assumed constant across its thickness and the convective heat flux is evaluated from the time rate of the slab temperature change. The use of this sensor with IR thermography is straightforward and either of the slab surfaces can be viewed by the infrared scanner. Furthermore, as for the heated thin foil, it is relatively easy to make the slab quite thin because the installation of a temperature transducer, such as a thermocouple or similar, is not required.

The *thin film* and *thin skin* sensor may be applied as an inverse method for material properties but just in two opposite borderline cases:

- Thermal disturbance that influence just the super-
  ficial layer of the body ($Bi >> 0.1$ or $Fo < 1/16$),
  in case of thin film;

- Uniform temperature across thickness ($Bi << 0.1$),
  in case of thin skin;

It's important to note that all the techniques are ap-
plied on a *slab*. Of course is not necessary apply the
method on a slab rather than a cylinder, but from the
mathematical and physical point of views the former is
much simpler than the latter. This is the reason because
the new method will be developed for a slab too.

3.2 New Methodology for Evaluation of Thermo-physical Properties

The need to develop a New Methodology for Evaluation of
Thermo-physical Property (METP) based on inverse heat
transfer comes from the evidence that not all the exper-
iments may be performed on a very thin slabs (to make
sure the Biot number smallness and so the no-dependence
of temperature on the slab thickness) or on semi-infinite
solids (to apply the simple mathematical formulation about
this case). Specially in the industrial applications or in
case of high temperature application, the Biot number
is too high to apply Thin skin techniques and the Fourier
number is also too high to apply the Thin Film technique.

In this work the author would like to develop the METP
that is able to perform measurement on the ceramic shell
sample in a wide range of temperature (up to $1000°C$) and
in case of $Bi \approx 0.1$.

In the Figure 3.1 is shown the modified Biot number in
dependence on the superficial temperature $T[K]$:

$$Bi^* = \frac{s}{k}\left(h + \sigma\varepsilon\left(T^2 + T_{inf}^2\right)(T + T_{inf})\right) \qquad (3.1)$$

for a slab in dependence on the material and on the wall
temperature. The coefficient h is the convective coeffi-
cient that is fixed (in this example $h = 10\ W/m^2K$), s
is the slab thickness, σ is the Stefan-Boltzmann constant,
ε the emissivity, k the thermal conductivity and T and
T_{inf} are respectively the wall temperature and ambient
temperature in Kelvin.

Material	k $[W/mK]$	ε
Ceramic	1	0.85
Oxide Stainless Steell	15	0.75
Platinum	70	0.10
Silver	420	0.10
Painted Silver	420	0.90

Table 3.1: Parameters setting for curves evaluation in Fig-
ure 3.1.

Since the temperature may be considered constant across
the thickness just in case of $Bi^* < 0.1$ (Mastrullo et al.
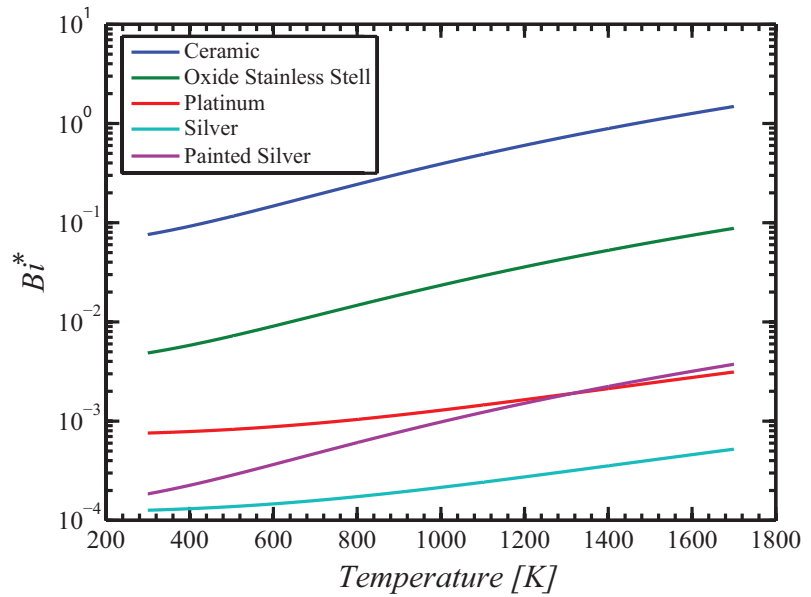
Figure 3.1: Bi^* for different slab material. The thermo-physical properties are kept constant and slab thickness s and ambient temperature T_{inf} have been fixed respectively equal to $1 * 10^{-2} m$ and $300 K$.

1991), the heated thin foil and thin skin sensors may not
be applied in the whole range of temperature in case of
ceramic materials. The Figure 3.2 shows the percentage
difference ΔT between the surface temperature and the
mean temperature across slab thickness in dependence on
the Fo and Bi^*. The deviation represent the percentage
error made considering the temperature uniform across
thickness at different *modified Biot number.*
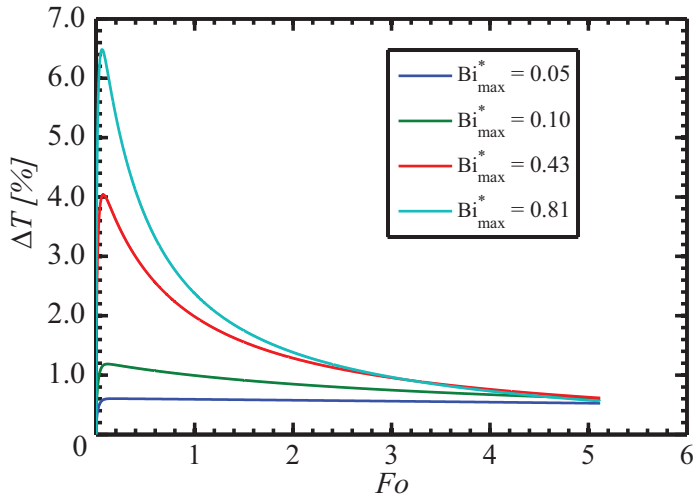
Figure 3.2: Percentage difference ΔT between the surface
temperature and the mean temperature across slab thickness
in dependence on the Fo and Bi^*. Bi^*_{max} is the Bi^* evaluated
at maximum temperature $T^*(Fo = 0)$.

Moreover the Fourier number will be much higher than
1/16 (the Fo range is [0-5]) such as the slab may not be
considered a semi-infinite solid and the thin film technique

may not be applied.

A numerical-experimental inverse method will be develop to overcome the limits imposed by the classical methods in order to find out the thermo-physical properties of the slab. As explained in the following paragraphs the thermo-physical properties of the Fourier differential equation will be varying to match the experimental time depending temperature of a ceramic slab heated over to $1000°C$ and cooled in quiet air. The results of the *curves approaching* are the slab thermo-physical properties.

The presented method can be also considered an inverse heat transfer method that involves both radiative and convection heat flux. A lot of inverse heat transfer method dealt with pure convection (Astarita & Carlomagno 2013) or radiation inverse heat transfer (Modest 2003). Just few works deal with the interaction between conduction and radiation (Park & Lee 2002) and very few works deal with the investigation of interaction between convection and radiation (Franca et al. 2001). Most of these investigations have concentrated on developing an inverse method using artificial data and mostly gray, constant-property media. This work deal with an inverse heat transfer method with the interaction of the convective and radiative heat flux on a media with temperature depending properties. Moreover the experiments are performed in a wide range of temperature.

For the sake of the clearness the most important technique innovations are summarize: the proposed METP is a *Non-Stationary* inverse heat transfer technique applied in a *wide range of temperature* in which both *convective*

and radiative heat transfer are involved and the thermal properties *depend on temperature.*

3.2.1   Mathematical Model

The physical model, Figure 3.3, takes into account an isotropic slab heated up to high temperature (about $1000°C$) that cools in quiet air at ambient temperature. In order to reduce the numerical cost of the heat conduction equation integration the mathematical model take into account just half slab (solid lines) even if the experimental runs will be performed on the whole slab (solids and dotted lines).

The Fourier differential equation for transient heat transfer without energy generation describes the cooling of a generic solid.

$$\nabla \cdot (k\nabla T) = C_v \frac{\partial T}{\partial t} \qquad (3.2)$$

where T in the temperature, k the thermal conductivity and $C_v = \rho c$ is the volumetric specific heat.

In case of a mono-dimensional slab (two dimensions much larger than the third) the eq. 3.2 becomes:

$$\frac{\partial}{\partial x}\left(k\frac{\partial T}{\partial x}\right) = C_v \frac{\partial T}{\partial t} \qquad (3.3)$$

where x typically is the coordinate across slab thickness.

Transient heat conduction in a slab with variable thermal conductivity has been of primary concern in many engineering applications. The problem arises because of existence of large temperature gradient in the solids which causes significant variation of the thermal properties of
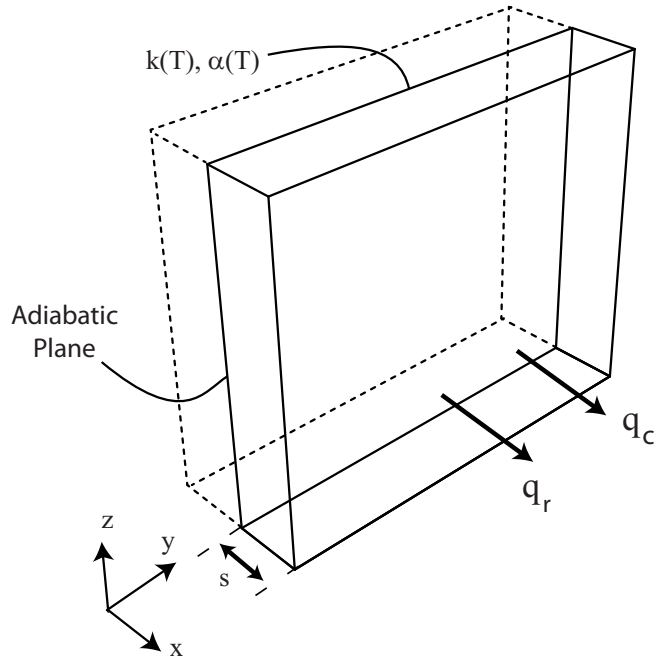
Figure 3.3: The slab is cooled by means of both radiative (q_r) and convective (q_c) heat flux through the two surfaces in correspondence with $x = s$ and $x = -s$. Of course numerical integration is performed just on the positive range of x. y and z dimension are much longer than x dimension s.

the materials. In the present case the difference between superficial temperature and the mean temperature across thickness may even be over 10%. The Figure 3.1 shows any curves in dependence on temperature and materials. The order of the maximum Bi^* is over 1 and the the curve $Bi^*_{max} = 0.81$ of the Figure 3.2 help us to define the order of the difference between mean and superficial slab temperatures: in the first step of the slab cooling the thermal properties of the materials may not be considered constant across slab especially because the method is ill-posed.

Any works deal with the numerical solution of the heat conduction in the case of variable thermal conductivity (Mishra et al. 2005, Su et al. 2009, Lin 1978) and because also the volumetric specific heat must be considered variable the eq. 3.3 is modified as (Lin 1978) proposes in his work:

$$\frac{\partial}{\partial x}\left(\alpha\frac{\partial T}{\partial x}\right) = \frac{\partial T}{\partial t} \tag{3.4}$$

The eq. 3.4 needs initial and boundary conditions to be analytically or numerically solved. The initial condition takes into account in this work is the most classical condition: uniform temperature T across thickness:

$$T(x,0) = T_{initial}; \quad \forall\, x \in [0, s] \tag{3.5}$$

where s is the semi-thickness value. Because the experiments will performed at high temperature both radiative and convective contribute have to be taken into account about the heat transfer at slab surfaces (Figure 3.6) and

the adiabatic plan has been fixed at $x = 0$ (Figure 3.7).

$$-k\frac{\partial T}{\partial x}(s,t) = h(T(s,t)-T_{inf})+\sigma\varepsilon(T(s,t)^4-T_{inf}^4); \quad \forall\, t > 0$$

(3.6)

$$\frac{\partial T}{\partial x}(0,t) = 0; \qquad \forall\, t > 0 \tag{3.7}$$

Of course the analytical solution of the 3.4, 3.5, 3.6, 3.7 does not exist. So a numerical method is necessary to solve the problem: to ensure a good solution the *PDE* method, provide by the program MATLAB, has been used (see Appendix C). In the equation 3.4 the unknown parameter is $\alpha = \frac{k}{C_v}$. Moreover it is not constant because the wide range of temperature and in particular:

$$k = k(T) \tag{3.8}$$

$$C_v = C_v(T) \tag{3.9}$$

and consequently:

$$\alpha = \alpha(T) \tag{3.10}$$

Also in the eq.3.6 the thermal conductivity k is an unknown parameter (see 3.8). In the general practice the thermo-physical properties are considered depending on the temperature by means of the interpolation polynomial. In particular the property p may be written down:

$$p\,(T) = p_0 + p_1 * T + ... + p_n * T^n \tag{3.11}$$

which is a *n-order* polynomial. In accordance with this widely used practical method the thermal diffusivity and thermal conductivity are expressed in terms of polynomial form. In this case the coefficient of the polynomial become the unknown parameters. In particular the eq. 3.8 and eq. 3.10 become:

$$\alpha\left(T\right) = \alpha_0 + \alpha_1 * T + \alpha_2 * T^2 \qquad (3.12)$$

$$k\left(T\right) = k_0 + k_1 * T + k_2 * T^2 \qquad (3.13)$$

The choice to truncate the polynomial at the second order comes from convergence considerations: a too high number of unknown parameters produce the instability of the inverse method. Of course it is not generally fixed the maximum number of parameters but it is necessary optimize the convergence quality against the polynomial correspondence with physical temperature dependence of the properties. In this case the author find out the optimization in the *2-nd order polynomial*.

The optimization process consists in an iterative changing of the unknown parameters on which the temperature in each point of the slab depends to minimize the functional error between the measured temperatures and the temperatures numerically generated by means of Fourier equation. Because the temperature is measured by means of an IR-camera, only the superficial temperature $(x = s)$ is compared during optimization process.

3.2.2   Dimensional Considerations

The mathematical model presented in the equations 3.3, 3.5, 3.6 and 3.7 depends on the following parameters:

$$t, T, T_{inf}, k, \alpha, s, x, \varepsilon, h$$

Because the thermo-physical properties depend on temperature a dimensionless form of them has been assumed untimely. Contrariwise the dimensionless temperature has been found out very useful for a fundamental reason: the polynomial coefficients of the thermal properties differ about any order of magnitude if polynomial is expressed such as in 3.12 and 3.13, but they are in same (or quite the same) order of magnitude if the temperature is expressed:

$$T^* = \frac{T - T_{inf}}{T_i - T_{inf}} \qquad (3.14)$$

Since the optimization procedure needs to estimate the polynomial coefficient it is much better work on parameter with the same order of magnitude. The choice allows to increase the method reliability and it is the key of the whole optimization process. Furthermore the x-coordinate has been normalised in reference to the semi-thickness s:

$$x^* = \frac{x}{s} \qquad (3.15)$$

With reference to the dimensionless terms 3.14 and 3.15, the mathematical formulation 3.3, 3.5, 3.6 and 3.7 becomes:

$$\begin{cases} \dfrac{1}{s^2}\dfrac{\partial}{\partial x^*}\left(\alpha\dfrac{\partial T}{\partial x^*}\right) - \dfrac{\partial T^*}{\partial t} = 0 \\[2ex] T^*(x^*,0) = 1; \qquad \forall\, x^* \in [0,1] \\[2ex] \dfrac{\partial T^*}{\partial x^*}(1,t) = \dfrac{hs}{k}(T^*(1,t)-1) + \dfrac{\sigma\varepsilon s}{k}T_{inf}^3(T^*(1,t)^4-1) \\[1ex] \qquad\qquad\qquad \forall\, t > 0 \\[2ex] \dfrac{\partial T^*}{\partial x^*}(0,t) = 0 \qquad \forall\, t > 0 \end{cases}$$

$$\text{(3.16)}$$

In this work the surface temperature numerically generated $T^*(1,t)$ will be shortly named T_n^* or, in its dimensional form, T_n.

An example of the temperature distribution in a generic slab has been numerically found out solving the equations 3.16 and an example is shown in Figure 3.4.

The optimization process consists in varying the unknown parameters on which the superficial temperature of the slab depends to minimize the objective function f defined as the norm of the differences between the measured temperatures T_m^*, and the temperature T_n^* generated numerically by the solution of 3.16:

$$f = \|T_m^* - T_n^*\| \qquad (3.17)$$

In order to make sure the technique properly works

Figure 3.4: Dimensionless temperature across thickness and depending on time. The classical convexity is shown and the maximum of temperature is always in correspendece with the adiabatic plan $x^* = 0$.

the use of a further, *unphysical* and unknown parameter is necessary. The delay parameter t_e introduces a translation of the numerical temperature curve. It is used to take into account two important facts:

- The initial time in which the model is exposed to ambient system is not known with precision;

- The slab must be extract from the furnace and the time spending to well positioning the slab is not

known with precision. Furthermore the extraction movement creates boundary conditions different in reference to the mathematical model;

With the use of the *delay* we consider heat transfer starting from an *unphysical* instant in which the slab cooling starts over the boundary conditions considered by the mathematical model.

3.2.3   Iterative Method and Convergence of Non-linear Minimization

The T_m^* drop is measured with the help of IR-camera. To estimate the thermo-physical properties in terms of their polynomial coefficients the following steps are followed:

1. Set all the known parameters:

   - Acquisition Frequency f_s;

   - Thickness s;

   - Initial Uniform Temperature $T^*(x^*, 0)$;

   - Ambient Temperature T_{inf};

   - Emissivity ε and Convective Coefficient h;

2. Set trial values to the unknown undergoing optimization;

3. Input surface temperature drop $T_m^*(t)$ to the optimization algorithm;

4. Run optimization procedure using the heat conduction problem 3.16 in order to generate the numerical temperature drop and the $T_n^*(t)$;

5. Compare T_n^* against T_m^* (recorded by means of IR-Camera) in order to estimate the unknown parameters;

In the numerical practice the method used to solve non-linear optimization problems is the *Levenberg-Marquardt* method (Levenberg 1944, Marquardt 1963), which is highly stable and reliable. Unfortunately, the so called *sensitivity coefficients* must be known in order to run the optimization. This kind of coefficients are derivatives of the numerical solution relative to the unknowns parameters. The Levenberg-Marquardt method would require the inefficient calculation of the sensitivity coefficient at each time step and at each iteration and is therefore better avoided. Hence the author has preferred to use optimization methods which do not require derivative calculation at each step; in particular, the optimizations methods used in the code is proposed by Moré & Sorensen (1983), *Trust-Region Methods*. The basic idea is to approximate the objective function f (eq. 3.17) with a simpler function q, which reasonably reflects the behaviour of function f in a *neighbourhood I* around the point i_0. This neighbourhood is the trust region. A trial step j is computed by minimizing (or approximately minimizing) over I. This is the trust-region subproblem:

$$min\ \{q(j)\ io + j \in I\} \qquad (3.18)$$

The current point is updated to be "i_0+j" if $f(i_0+j) < f(i_0)$; otherwise, the current point remains unchanged and I, the region of trust, is shrunk and the trial step computation is repeated.

3.2.4   Numerical Validation and Noise Influence

A full numerical validation has been carried out for the optimization problem presented in the par. 3.2.3. The purpose of the numerical validation is to verify that the method works and the noise influence on the estimation of *Thermal Diffusivity* and *Thermal Conductivity* as meaningful parameters characterizing each temperature drop. The noise is an experimental disturbance that occurs during experimental data acquisition due to the instrument imperfections.

Hence a perfect numerical temperature drop may be *noised* by means of the addition of random noise in order to simulate the actual signal. The noise must have a Gaussian distribution characterized by zero average and variance equal to the instrument signal noise. The IR-camera used in this work is the FLIR S65 and its characteristics, included signal noise at high temperature, have been presented in par. 2.7.1. In the Figure 3.5 a numerical noised curve is shown.

Because the noise is a random occurrence the method has be applied on a large number ($n = 900$ in the present case) of noised curves with n different distribution of noise. Running the inverse procedure over the n curves the re-
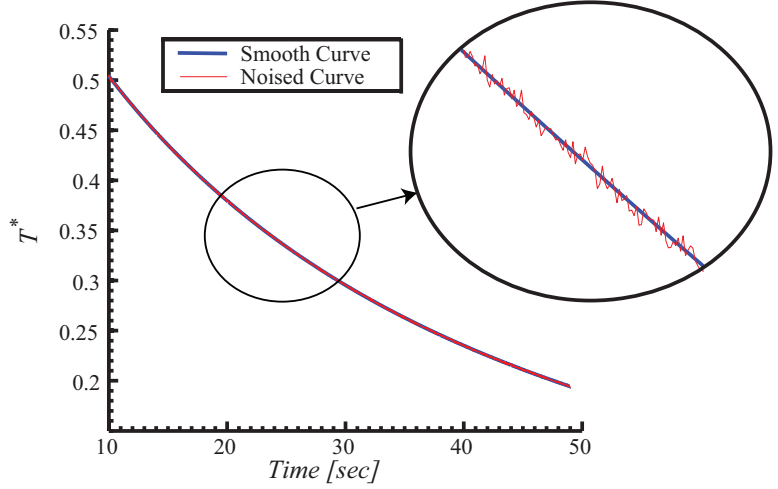
Figure 3.5: The noise of the FLIR S65 has been added to the smooth curve.

sults (in terms of thermo-physical properties) will be always different.

If $w(T)$ is the exact value (used to build the curves) of the parameter to estimate, $w_i(T)$ the value of that parameter as estimated in the generic optimization i, the mean value $\overline{w}(T)$ is defined as

$$\overline{w}(T) = \frac{1}{n} \sum_{i=1}^{n} w_i(T) \qquad (3.19)$$

and the standard deviation $\sigma(T)$ like as:

$$\sigma(T) = \sqrt{\frac{1}{n} \sum_{i=1}^{n} (w_i(T) - \overline{w}(T))^2} \qquad (3.20)$$

The standard deviation over the n measurements represents the standard deviation of the proposed method and it may be applied to evaluate the interval of confidence in case of m samples $(m < n)$. In general in the experimental test runs at least 30 curves, in correspondence with 30 independent points, are recorded and in this case $m = 30$. Of course the value of m is not fixed and it may be varied.

Hence the average value over the m samples is evaluated as:

$$\overline{u}\left(T\right) = \frac{1}{m}\sum_{i=1}^{m} w_i\left(T\right) \qquad (3.21)$$

and the exact w value will be in the interval:

$$\left[\overline{u}\left(T\right) - Z_{C\%}\sqrt{\frac{\sigma^2}{m}}, \overline{u}\left(T\right) + Z_{C\%}\sqrt{\frac{\sigma^2}{m}}\right] \qquad (3.22)$$

with a confidence depending on the factor $Z_{C\%}$. In particular $Z_{C\%} = 1.96$ in case of confidence level equal to 95%.

In the Figure 3.6 and Figure 3.7 the standard deviation is plotting in reference to the temperature, respectively for *thermal diffusivity* and *thermal conductivity*. In particular it is represented as a percentage of the ratio $\sigma\left(T\right)/w\left(T\right)$, where $w\left(T\right)$ is the exact value of the parameter to estimate.

Furthermore the method shows a *bias error* evaluated like as:

$$\beta\left(T\right) = \overline{w}\left(T\right) - w\left(T\right) \qquad (3.23)$$

and it is also plotted the same figure in reference to the temperature.
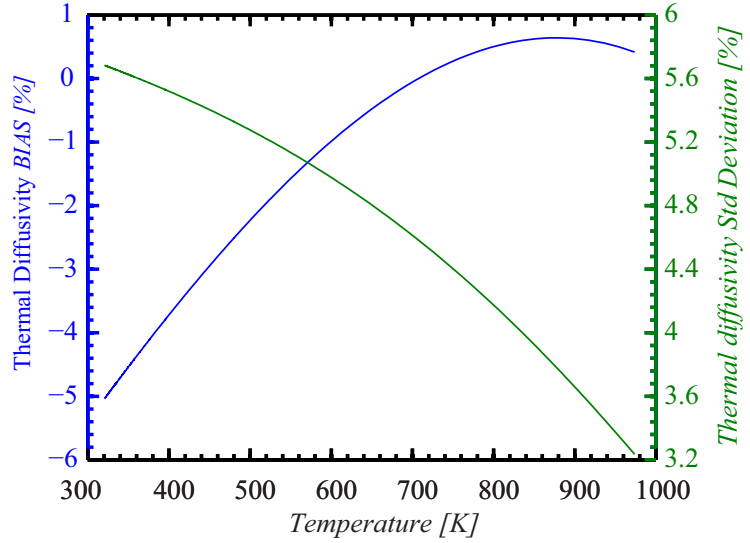
Figure 3.6: Thermal diffusivity: bias error and standard deviation in dependence on the temperature.

As a rule, the method provides the most accurate results at high temperature and it happens because the noise/signal ratio becomes lower as the temperature increases. In particular the camera noise causes a maximum bias error at lower considered temperature of 5% and 2% and a standard deviation of 6% and 1% respectively on
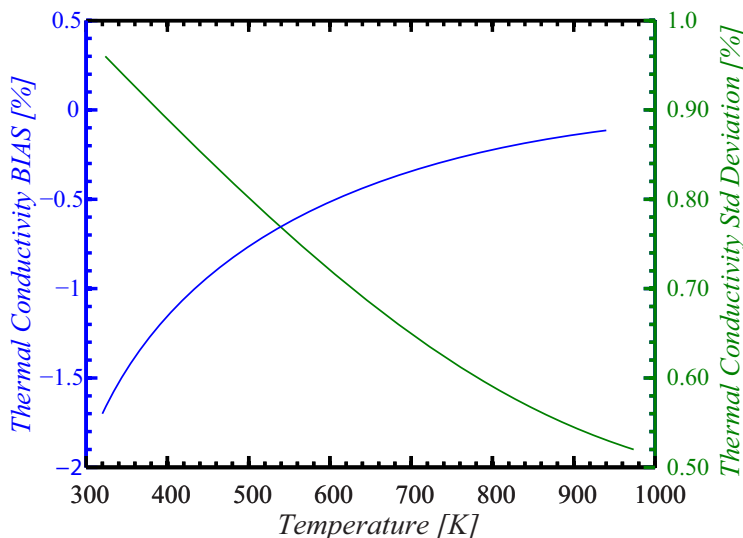
Figure 3.7: Thermal conductivity: bias error and standard deviation in dependence on the temperature.

the thermal diffusivity and thermal conductivity. The results point out a good reliability of the METP especially if it is considered that inverse method are generally too much sensitive on the signal noise.

The above analysis has been performed fixing any parameters. The *thermal diffusivity* and *conductivity* are fixed equal to the MACOR properties (see Appendix A) and the other parameters are fixed as specified in the 3.2: and These are the standard parameters and for the experimental test running performed in this work. Hence

Property	Value
Initial Temperature	$1300K$
Acquisition Frequency	$50Hz$
Slab Thickness	$3mm$
Emissivity	0.80
Convective Coefficient	$10W/m^2K$
Ambient Temperature	$300K$

Table 3.2: Parameter used for estimate the reliability of the method in reference to the noise diturbance.

the analysis may be repeated if the experimental conditions vary in order to the reliability of the noise influence.

3.2.5   Sensitivity Analysis

Of course the signal noise is not the unique source of error and further variables have to be token into account. In particular the uncertainty and uncertainty propagation of any parameters have to be analysed and it is because the sensitivity analysis has been performed in order to resolve this kind on problem.
The input parameters that are token into account for the sensitivity analysis are:

- Convective Coefficient h;

- Thickness s;

- Initial Temperature T_{ini};

- Emissivity ε;

In reference to the rule *UNI CEI ENV 13005* the sensitivity coefficient are find out. For the sake of the completeness the technical meaning of the sensitivity coefficient is summarize. If a general quantity of a parameter Y may be expressed in dependence on n variables:

$$Y = f(x_1, ..., x_n) \tag{3.24}$$

the sensitivity coefficient of Y with respect to the $j-th$ variable x_j is:

$$C_{xj} = \frac{\partial Y}{\partial x_j} \tag{3.25}$$

Thermal diffusivity sensitivity coefficients

Thermal conductivity sensitivity coefficients
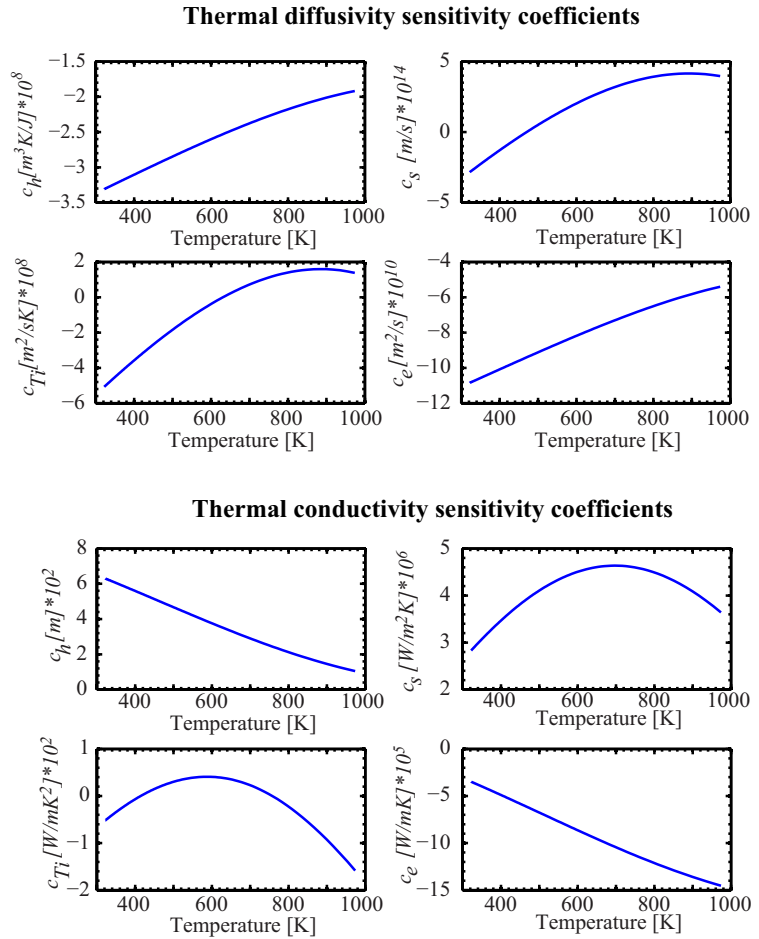
Figure 3.8: Thermal diffusivity and thermal conductivity: sensitivity coefficients.

Sensitivity coefficients describe how the measurement of Y would be influenced by small changes in the generic input parameter x_j. Hence the uncertainty U_Y about Y may be evaluated in reference to the uncertainties u_{xj} about x_j:

$$U_Y = \sum_{j=1}^{n} C_{xj} u_{xj} \qquad (3.26)$$

The Figure 3.8 shows the sensitivity coefficient for thermal diffusivity and thermal conductivity. In particular C_h, C_s, C_{Ti} and C_e are respectively the sensitivity coefficients to the convective coefficient h, thickness s, initial temperature T_i and emissivity ε. These coefficients are needful to find out the total uncertainty of the proposed method and they will be used in the experimental application in order to evaluate the error in the parameters estimated. The error estimated by means of the eq. 3.26 must to be added to the uncertainty due to the noise.

3.3   Conclusion

In this chapter, the new inverse heat transfer method has been presented and validated numerically. The results of the validation have shown how the technique can reliably be used in order to evaluate the thermo-physical properties of a generic slab. Furthermore its stated goals to allow accurate measurements in presence of finite delay and to improve its performance in terms of sensitivity to parameters measurements errors have been met.

In reference to the criteria proposed by Beck (1985) and reported in *Appendix A* the inverse heat conduction procedures has been analysed.
In particular:

- Point **1** essentially means that the method has to find out reliable results if should be perform an *auto-validation*: validation on temperature curves without error. In this case the method does not point out any problem to find out the parameters to estimate;

- Points **2** and **16** are strictly correlated in this work because the sensitivity analyse 3.2.5 points out that measurement errors influence on the output (numerically evaluated) is acceptable in the range of usual experimental error;

- Points **3** and **7** are met in that the use of IR-camera with any frequency of acquisition is allowed. Furthermore the number of the observation does not limit the method capabilities, even if the the observations may not overcome the 100'000 samples in order to contain computational costs;

- Point **5** is met because the mathematical model and methodology on which the method is based and the appropriate choice of optimization routines avoid the use of the derivative terms;

- The use of the parameter delay allows to meet point **6** because the sensor works without knowing the ex-

act moment in which the ceramic sample starts cooling;

- Finally, the use of infrared thermography makes point **4** not relevant in this work. Furthermore the material on which the METP has to work is well established and point **8** does not have interest.

- Point **9** is the best goal of this method and of course it is met;

- the method algorithm may be easily ran on a common PC and it is the goal of point **12**. Since the algorithm is based on simple MATLAB tools that may be easy handled and the geometry of the model may be very easily changed among *slab, cylinder* and *sphere* points 11, 13, 14 are also met;

- Contact conductances and different surface heating/ cooling have not been considered, but they can be easily implemented (points **10** and **15**);

Ultimately the author may consider the inverse heat transfer method such as a reliable method.

Chapter 4

Experimental Test Running

In the paragraph 3.2.1 has been introduced the mathematical model about heat conduction integration problem about an isotropic slab under-posed to convection and radiative boundary conditions (3.3, 3.5, 3.6, 3.7, 3.16). In particular the right hands of the 3.5 and 3.6 are considered known, in other word the METP needs to know the *heat flux* and it is completely known if the temperatures are known and the convective (h) and radiative coefficients (emissivity ε) are known.

The following two paragraphs deal with the estimation of these coefficients by means of literature survey or experimental testing.

Furthermore the experimental apparatus has been presented and any experimental tests on ceramic materials have been performed in order to experimentally validate

79

and to apply on a real case the METP. The ceramic material tested are respectively MACOR and ceramic self-made by E.M.A. S.p.A. through the industrial shelling procedure.

4.1   Free Convection on a Vertical Plate

In order to solve the heat conduction problem (3.16) any parameters must be known. The convective coefficient h is one of them. In the present case the motion of the air arises "naturally" and the related convective mode is termed *natural convection*.
The natural convection on a vertical plate may be grouped in two main categories: Uniformly Wall Temperature (UWT) and Uniformly Wall Heat Flux (UWF). A lot of works deal with the natural convection and in particular free convection on a vertical slab is one of the most studied topics in heat transfer science. Hence many correlations are available in literature both for the former group (Bhavnani & Bergles 1990, Cairnie & Harrison 1982, Havet & Blay 1999, Ostrach 1953, Tsuji et al. 2007) and the latter group (Sparrow & Gregg 1956, Aydin & Guessous 2001, Aydin 97, Chang & Lee 2008); furthermore more accurate studies about the natural convection phenomena are available (Gebhart 1973, Martynenko et al. 1984, Chen & Eichorn 1976). The present case may be considered like as UWT natural convection category. The main correlations have

the following mathematical form:

$$Nu_y = C_1 \left(Gr_y\right)^{n1} \left(Pr\right)^{n2} \tag{4.1}$$

in which Nu_y and Gr_y are respectively the Nusselt number, eq. 4.2, and Grashof number, eq. 4.3, based on the y-coordinate (Figure 3.3), Pr is the Prandtl number, eq. 4.4, referred to the air at film temperature and C_1, n_1 and n_2 are the parametric coefficients.

$$Nu_y = \frac{hy}{k_{air}} \tag{4.2}$$

$$Gr_y = \frac{g\beta y^3 \left(T_{wall} - T_{inf}\right)}{v^2} \tag{4.3}$$

$$Pr = \frac{\mu c_p}{k_{air}} \tag{4.4}$$

For the sake of completeness it is point out that:

$$Ra_y = Gr_y Pr \tag{4.5}$$

The following table summarize the coefficients in reference to the author and, in the last row, are summarized the coefficients that better fit the correlations token into account. The *Best Fit Coefficients* are used in this work to estimate the convective coefficient h over the ceramic sample. In the table 4.1 are reported just the coefficients for the laminar natural correlations that occurs if $10^3 < Ra_x < 10^9$. It is because it has been verified that air motion around slab is always in laminar state during experimental tests. Finally it is important to point out

Reference	C_1	n_1	n_2
Havet & Blay (1999)	0.357	0.25	0
Chen & Eichorn (1976)	$f(Pr)$ [1]	0.25	0.25
Ostrach (1953)	0.355	0.25	0
Gebhart (1973)	0.355	0.25	0
Best Fit	0.387	0.25	0

Table 4.1: Correlation coefficients in relation with eq. 4.1.

that the air thermo-physical properties must be evaluated at film temperature, defined like as the average between wall temperature and ambient temperature.

4.2 Test Slabs Emissivity

In addition to the convective heat transfer coefficient it is necessary to know the emissivity in order to completely define the heat flux. The emissivity depends on a lot of parameters (more than convective coefficient) such as temperature, angle of view, wavelength and surface finishing. An high surface roughness without preferential directions increases the emissivity and make it less sensible on the angle of view. As a consequence it is not always possible to determine the emissivity of a body and in many cases the best way to evaluate the emissivity is the experimental measurement.
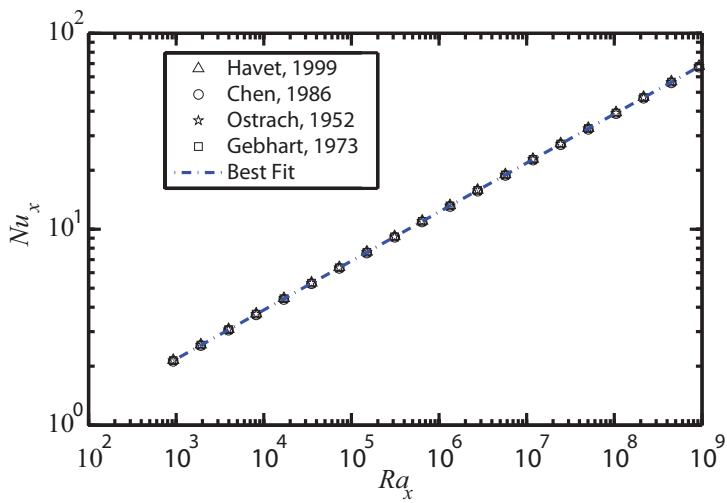
Figure 4.1: Nu_x dependence on Ra_x on an iso-thermal vertical plate.

4.2.1   MACOR Emissivity

MACOR is a widely used material in research field and
its properties are available in many works (Cardone et al.
2012). Hence the emissivity is evaluated by means of lit-
erature survey. The Figure 4.2 shows the directional emis-
sivity of MACOR even if in the present work will be just
used the normal emissivity.
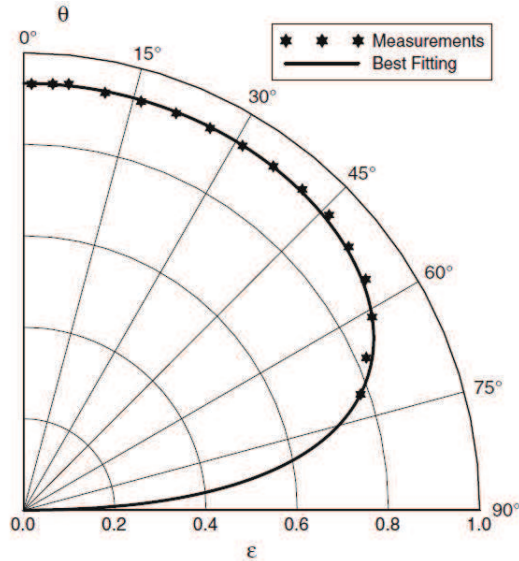
Figure 4.2: Directional emisperical emissivity of MACOR.

The data allow to fix the normal emissivity at $\varepsilon =$
0.934. In fact the best fit has the following parametric

form:

$$\varepsilon = \varepsilon_0 \left(\cos\theta\right)^{\frac{a}{(\cos\theta)^b}} \qquad (4.6)$$

in which $\varepsilon_0 = 0.934$, $a = 9.8x10^{-3}$ and $b = 2.4$ have been found out by means of a minimization procedure between experimental results and eq. 4.6 by Cardone et al. (2012).

4.2.2   EHT Shell System Emissivity

The experimental test has been also performed on a ceramic slab self-made by EMA. The ceramic is the *EHT shell system* (in the following just EHT). There are no information about this material in the literature documentations, but a literature survey about similar material has been made. In particular Touloukian (1967) dealt with any similar materials, like as *mullite*, and he gave any fundamental informations that are resumed in the Figure 4.4.
Furthermore an experimental test has been necessary in order to estimate the *EHT emissivity*. The experimental apparatus, shown in Figure 4.3, is essentially composed by:

- Ceramic Sample;

- Furnace;

- IR-Camera, FLIR S65;

- Dual Color Pyrometer, LAND M780;

Figure 4.3: Experimental apparatus for EHT emissivity measurement.

- PC acquisition system;

The IR-camera characteristics are resumed in par. 2.7, Table 2.1. The pyrometer characteristics are resumed in the Table 4.2.

The use of the dual color pyrometer provides two important measurements: the first one is the absolute temperature T, using the dual color mode, the second one is the emissivity at $1\mu m$, using the monochromatic mode. Of course the pyrometer may work on both modes at the same time. The absolute temperature is used to find out the emissivity averaged over spectral range of the IR-

Property	Value
Spectral Range	Two Narrow Band Near $1\mu m$
Resolution	$1K$
Accuracy	$\pm 0.5\%$ of full scale
Temperature Range	$750 - 2000°C$
FOV ratio	$1/90$

Table 4.2: Dual color pyrometer LAND M780. Technical characteristics.

camera by mean of the eq. 4.7:

$$\varepsilon = \frac{I}{R}\left(e^{(B/T)} - F\right) \qquad (4.7)$$

in which I is the IR-camera signal like as defined in eq. 2.12 and R, B and F are the IR-camera calibration constants.

The experimental data are acquired during ceramic cooling from high temperature ($1200°C$), reached by means of a furnace, down to ambient temperature.

The Figure 4.4 shows that this kind of materials have a step-like in monochromatic emissivity in the neighbourhood of $4\mu m$. Also the experimental results are in good agreement with the literature survey and, in order to estimate the normal total EHT emissivity, the eq. 2.7 about total emissivity may be applied under the condition:
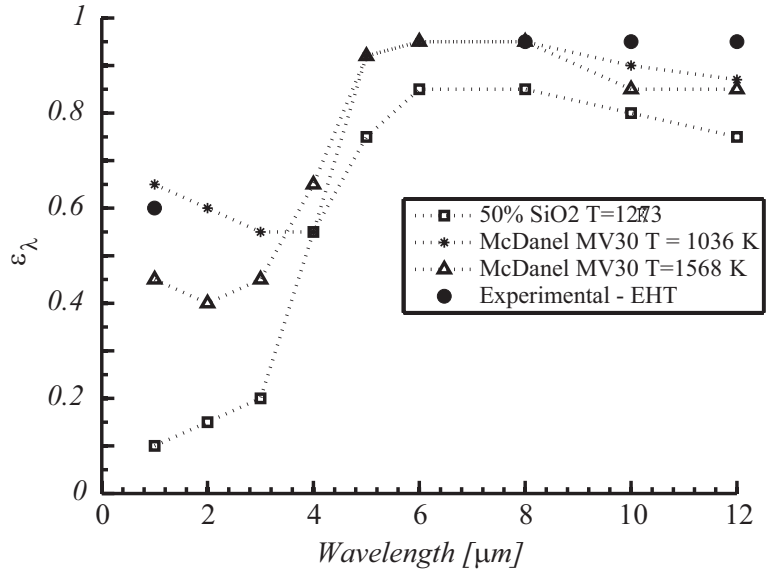
Figure 4.4: Mullite. Data from Touloukian (1967) and from experimental results.

$$
\begin{cases}
\varepsilon_\lambda = 0.60 & \lambda < 4\mu m \\
\\
\varepsilon_\lambda = 0.95 & \lambda > 4\mu m
\end{cases}
\tag{4.8}
$$

in the integration range $[0.1 - 13\mu m]$. The integration must be repeated varying the temperature in order to find out the emissivity dependence on the temperature. Hence the emissivity dependence on the temperature is the consequence of the *Wien's law* more than the monochromatic emissivity dependence on the temperature.

The Figure 4.5 shows the integration result in which a

polynomial law of the emissivity is reported. The polynomial form has been used in order to include the emissivity dependence on the temperature in the METP algorithm:

$$\varepsilon\left(T\right) = 0.8953 + (5.001 * 10^{-4}) * T - (1.29 * 10^{-6}) * T^2$$
$$+ (8.531 * 10^{-10}) * T^3 - (1.844 * 10^{-13}) * T^4$$

$$(4.9)$$
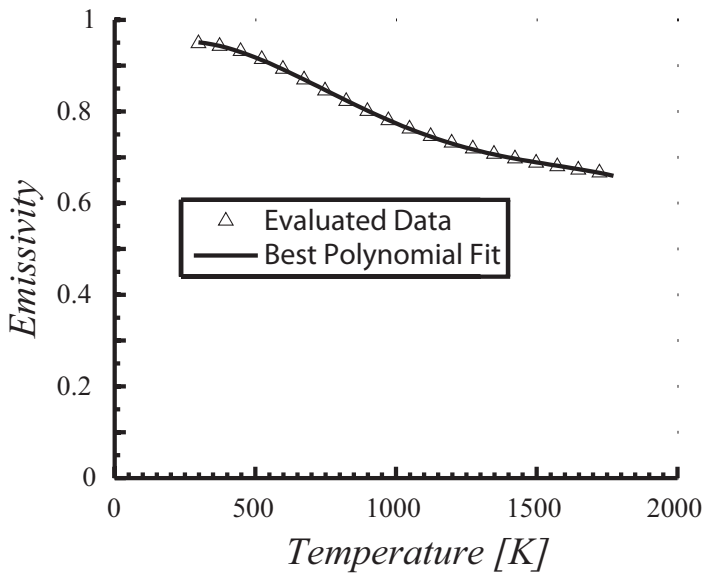
Figure 4.5: Emissivity evaluation of the EHT shell system.

4.3 Experimental Validation

One of the most important kind of validation is the *experimental validation*: it is the most widely used method in which the solution is compared against the literature data or data sheet of a well known material. This method plays a key role because it provides a direct evidence of the model consistence.

In the present work the experimental validation has been performed on a MACOR sample (see Appendix A) because it is one of the best known material both in mechanical and in thermo-physical properties.

In order to perform the IR-recording on the MACOR slab cooling from high temperature down to ambient temperature an *ad-hoc* experimental apparatus has been built. It must essentially allow the slab heating up to $1000°C$ and the slab cooling under the boundary conditions expressed in the eq. 3.16.

The experimental apparatus (4.6) is composed by:

- *IR-camera* (see par. 2.7);

- *Furnace*, it is a *Carbolite* furnace and the maximum operating temperature is $1100°C$;

- *Thermocouple*, it is a *type K* thermocouple and it is positioned as close as possible to the slab in order to record the cooling initial temperature. The temperature range is $[0 - 1370°C]$ with an accuracy of $\pm 1°C$. One more thermocouple has been used to record ambient temperature;
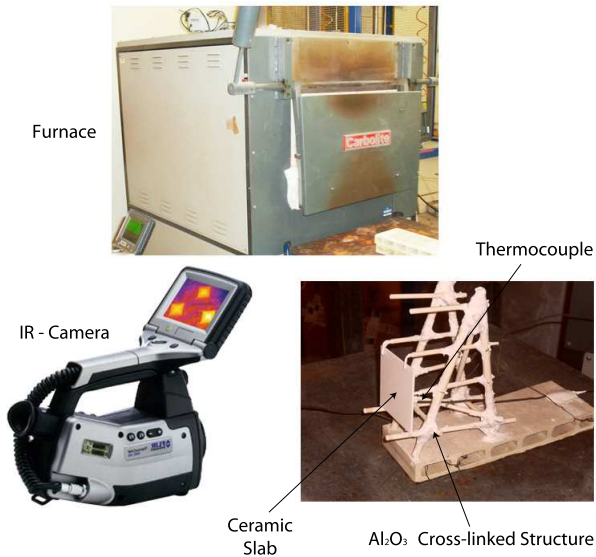
Figure 4.6: Experimental apparatus.

- *Support Structure*, that must keep vertical the slab
  and it must withstand at high temperature. It is a
  self-made cross-linked structure in Aluminium oxide
  (Al_2O_3);

- *PC acquisition system*, it records all the data;

The Figure 4.7 shows an IR frame of the MACOR slab
during cooling. The slab may be considered at uniformly
temperature (UWT conditions).
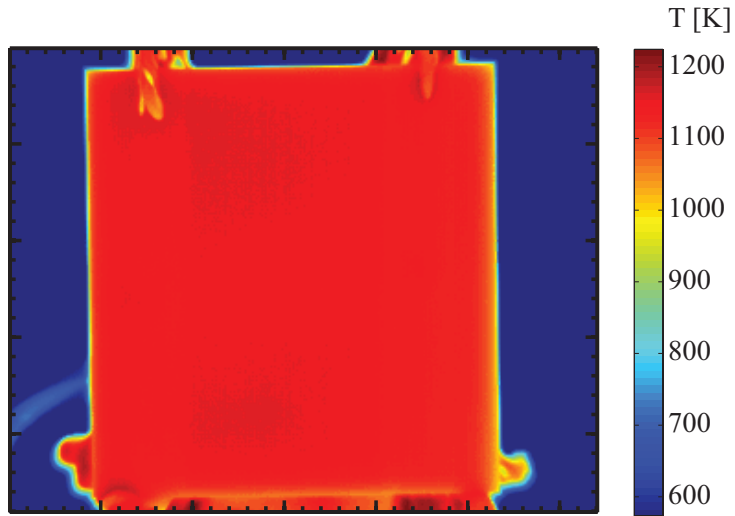
Figure 4.7: IR thermogram of the macor slab.

The maximum temperature is limited by the material: in fact MACOR withstands up to $1000°C$ (without load). The temperature drop of thirty random points over the slab is recorded and analysed by means of the METP algorithm and the results of the procedure are shown in the Figure 4.8 (*thermal diffusivity* and(*thermal conductivity*). The data are the average over the thirty points analysis and the values are reported in the figures (*METP* is linked to the experimental results). Furthermore the error bars are built in reference to the confidence level of 95% at which has been added the error due to the sensitivity coefficients, defined in par. 3.2.5.
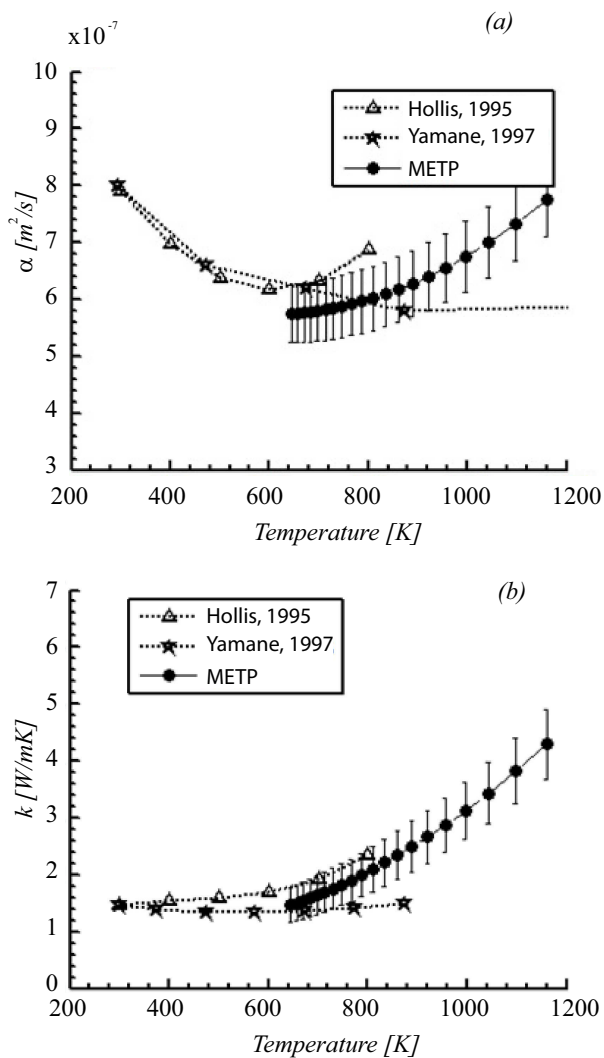
Figure 4.8: Results of the minimization procedure about *(a) thermal diffusivity* $\alpha[m^2/s]$ *and (b) thermal conductivity* $k[W/mK]$. The METP value are the average over 30 points.

For the sake of completeness an example of experimental curve and its numerical prediction (plotted with the optimized thermo-physical properties) is shown in Figure 4.9. The solid line represents the experimental temperature drop while the dotted curve represents the numerical optimization result. Note that also delay time is an output of the inverse process and it is an *unphysical delay*, such as defined in par. 3.2.2, that takes into account the time spending in order to extract the slab from furnace and any different and unpredictable boundary conditions during extraction movement.
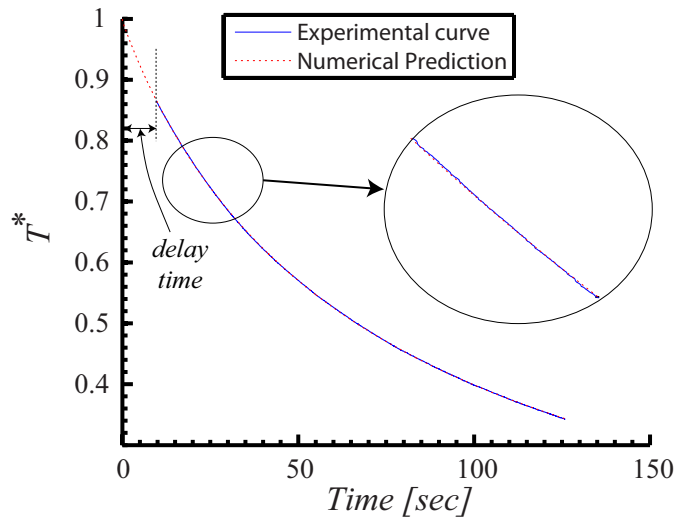
Figure 4.9: Experimental curve compared with the optimization curve built using the thermo-physical properties found out at the end of the oprimization process. Also the delay time is shown such as a delay in the recording of the temperature.

4.4   EMA Real Case

The METP has been performed on an EHT-ceramic sample made on purpose by means of the shelling process in EMA. In order to put into practice the technique a

Figure 4.10: Cross-linked structure with EHT slab.

test running on an EMA self-made ceramic has been performed.

The ceramic is the EHT shell system and the ceramic slab has been arranged like as the MACOR slab onto the experimental apparatus (compare Figure 4.6 Figure 4.10). In this case the maximum temperature of the test running is limited by the furnace ($1100°C$). The Figure 4.11 shows the *thermal diffusivity* curve and *thermal conductivity* curves. The data denoted like as *"Reference x"* are

provided by EMA company and in compliance with the copyright the y-axes are normalized in reference to an arbitrary value.
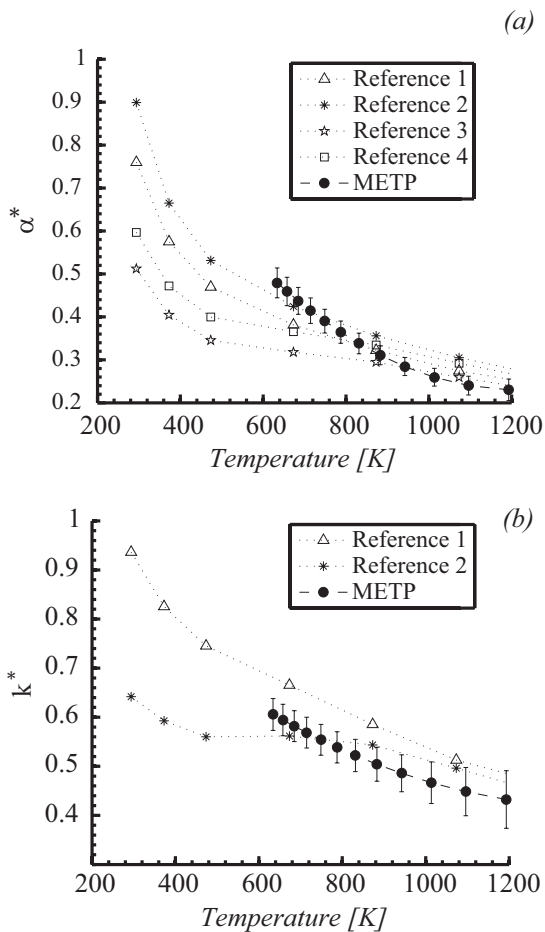
Figure 4.11: Results of the minimization procedure about *thermal diffusivity (a)* and *thermal conductivity (b)* on EHT ceramic slab. The y-axes has been normalized in reference to an arbitrary value in compliance with the EMA rights.

4.5   Conclusion

New Methodology for Evaluation of Thermo-physical Property (METP), in which both convective and radiative effects are considered, has been experimentally validated and applied on a real case.

In order to numerically validate the METP proposed in *chapter 3*, it has been used to evaluate the thermo-physical properties, in terms of *thermal diffusivity* and *thermal conductivity*, of a well known ceramic material (MACOR): the experimental validation has been performed and the results are compared against the data from literature survey. The METP has proved to be extremely stable, even in presence of significant noise, and the comparisons with the data of MACOR shows that the METP has been capable to provide good accuracy.

It's important to note that the thermo-physical properties of ceramic materials have been evaluated in dependence on temperature and in a wide range of temperature with a fast procedure that allows to save both time and money. The METP is applied on a real EMA case, in which a ceramic EHT slab is used like a ceramic sample. In order to run the optimization algorithm all the characteristics that define the heat flux have to be known. It is because a preliminary analysis (literature survey or experimental testing) on the emissivity and convective coefficients of the ceramic slab has been done. Even if the data are in general agreement with the data provided by EMA, the accordance in not so good such as in case of MACOR. The discrepancy is essentially due to the uncertainty about

EHT emissivity. In fact the emissivity has been partially evaluated by means of experimental tests and completely estimated by means of a comparison with similar materials (e.g. mullite) behaviour.

Any experimental problems has been encountered, in particular the difficulty about the slab extraction from the furnace that has caused an high number of experimental test running. The difficulty may be solved by means of a specific design of furnace and extraction method.

Chapter 5

Conclusion

In the investment casting process, as a rule, the wax pattern (disposable specimen in the shape and size of the final product) is invested into ceramic slurry followed by the application of a coating of dry refractory particles (*stucco*) which, when dried, gives a thin refractory shell.

The application of slurry and stucco is repeated, with drying between each successive coat, until the shell mould of sufficient thickness is achieved. Following completion of shell build, de-waxing and shell hardening processes get ready the shell for the following pouring of the molten metal into the expendable ceramic mould. The production of the investment casting ceramic mould is a crucial part of the whole process. The use of an expendable pattern confers an unique advantage to the investment casting process because the pattern is removed from the mould without any disturbance of the latter, but the continuous shell changing produces a random changing on the bound-

ary conditions that directly affect the casting success. A
new experimental/numerical methodology for evaluation
of thermo-physical properties based on inverse heat trans-
fer (METP) has been developed and validated. Of course
a lot of methodologies may be applied in order to achieve
this goal, but the purpose of the present work is the de-
velopment of a new fast method that is a *Non-Stationary*
inverse heat transfer technique applied in a *wide range of
temperature* in which both *convective and radiative* heat
transfer are involved (and known) and the thermal prop-
erties (the unknown parameters) must be find out in *de-
pendence on the temperature.*

The METP is based on a simple mathematical descrip-
tion of a slab heat transfer that exactly is the heat con-
duction problem described by the parabolic differential
equation (Fourier's equation) completed by properly ini-
tial and boundary conditions. In particular, given the
effects (time variation of surface temperatures and heat
fluxes) the causes (the material properties) must be es-
timated. Inverse problems are typical ill-posed problems
since the solution can be extremely sensible to the noise
and can be unstable. Hence a numerical validation has
been performed in order evaluate the noise instrument in-
fluence on the reliability and repeatability of the METP.
Besides the sensitivity analysis of the results has been per-
formed in order to estimate the uncertainty propagation
of any fundamental parameters, e.g. emissivity, thickness,
initial temperature and convective coefficient. The results
of the numerical validation show that the METP may be
considered such as a reliable method.

The further steps deal with the application of the METP on real cases. First of all the experimental validation is performed in order to provide a direct evidence of the model consistence. In particular METP has been applied on the MACOR ceramic: the surface temperature of a MACOR slab has been measured by means of the IR-thermography during cooling from $1000°C$ down to ambient temperature. The temperature of at least 30 slab points have been processed by means of METP and the results compared against the literature survey about MACOR thermo-physical properties. The METP, in the limits of its evaluated errors, is in good agreement with literature survey and it is because the method may be considered *experimentally validate.*

Furthermore the METP is applied on self-made material by EMA (EHT-ceramic) and in this case, even if the data are in general agreement with the data provided by EMA, the accordance in not so good such as in case of MACOR. The discrepancy is essentially due to the uncertainty about EHT emissivity. In fact the emissivity has been partially evaluated by means of experimental tests and completely estimated by means of a comparison with similar materials (e.g. mullite) behaviour. Because METP has to be applied on EMA ceramic material a full evaluation about emissivity has to be performed, but this topics is beyond the purpose of this thesis.

Then new methodology for evaluation of thermo-physical properties proposed in this work has proven to be accurate and stable and applicable in the test configuration presented in the previous chapters.

Appendix A

MACOR®'s Properties

Figure A.1: MACOR® in its classical appearance.

MACOR® is a white porcelain-like (in appearance) material composed of approximately 55% *fluorophlogopite mica* and 45% *borosilicate glass*. The material contains the following compounds (Approximate Weight percentage):

- Silicon - SiO_2 : 46%;

- Magnesium - MgO: 17%;

- Aluminium - Al_2O_3: 16%;

- Potassium - K_2O: 10%;

- Boron - B_2O_3: 7%;

- Fluorine - F: 4%;

Unlike ceramic material used in the investment casting process 1.3, MACOR ceramic material has the particular characteristic to have no porosity.

The most interesting characteristics of these kind of ceramic are provided by the mica. Micas are a group of sheet silicate minerals strong, flexible and cleavable in nature (Mustafa 2001). They comes in several forms including *muscovite*, *biotite*, and the lesser-known *phlogopite* variety. Micas are used to provide easy paths for crack propagation in some commercial machinable ceramics (Carter & Norton 2007). The borosilicate glass is often used like as a binder. The reason of the author's interest about MACOR is simply explained: MACOR is widely used in the scientific field and its properties and the properties dependence on the temperature are well known. Hence a sample of macor ceramic may be used in order to experimentally validate the new heat flux sensor explained in the following of the work. The Figure A.2 ,Figure A.3 and Figure A.4 show the MACOR thermo-physical properties in dependence on the temperature.

Furthermore a Differential Scanning Calorimetry (DSC) analysis has been performed by means of PL-STA1500HF
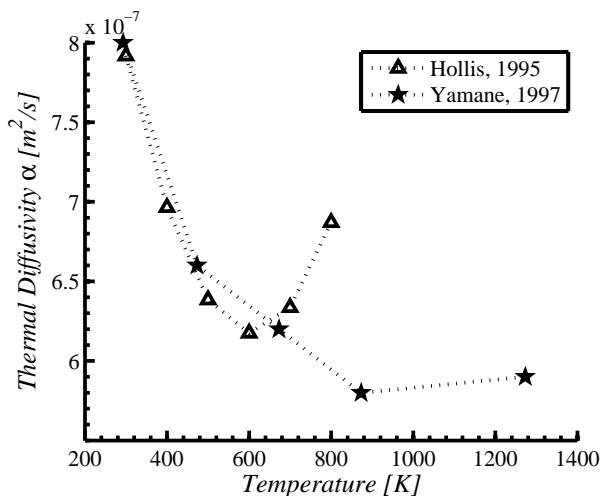
Figure A.2: Thermal Diffusivity of MACOR by (Hollis 1995) and (Yamane et al. 1997).

DSC Analyser over a wide range of temperature ($30^oC -$ 1100^oC). The Figure A.5 shows any steps in Temperature-Heat Flux curve that point-out any glass transitions (endothermic transformations). In correspondence with the temperature $T = 1000^oC$ is clearly shown a transition phase (Höhne et al. 2010). In fact the maximum operating temperature (without load) has been fixed to 1000^oC by the Corning. The DSC analysis had been performed on a macor sample (about $57mg$) under-posed to a controlled temperature ramp ($20K/min$) from ambient temperature up to 1100^oC.
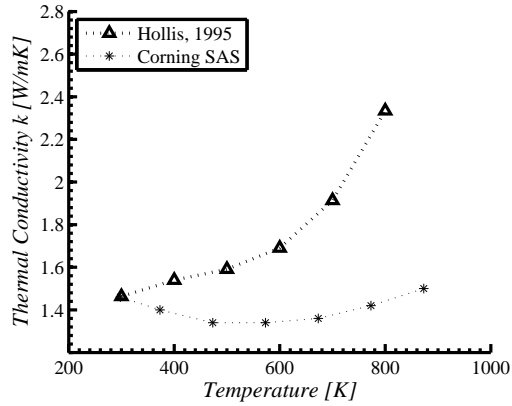
Figure A.3: Thermal Conductivity of MACOR by (Hollis 1995) and Corning data sheet.
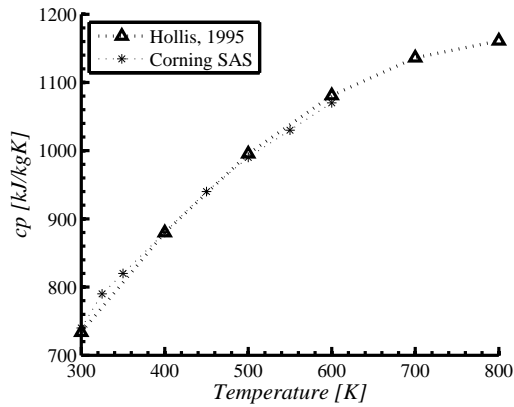
Figure A.4: Specific heat capacity of MACOR by (Hollis 1995) and Corning data sheet.
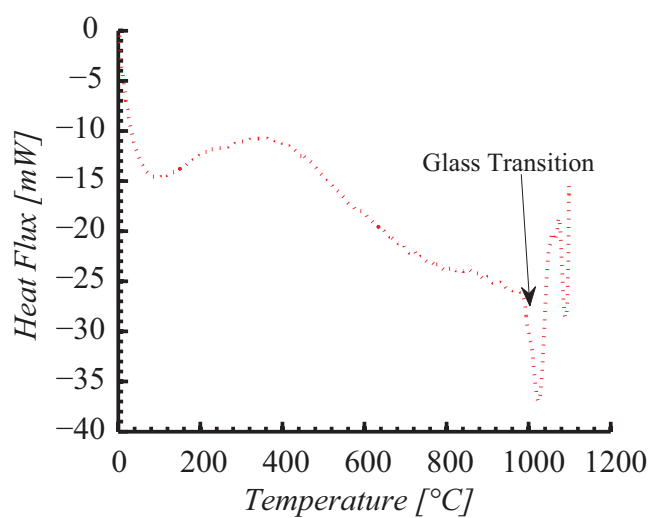
Figure A.5: Heat Flow on MACOR sample performed by DSC analyser PL-STA1500HF.

Appendix B

Beck's Criteria

Beck (1985), in his work *"Inverse Heat Conduction. Ill-posed Problems"*, proposed any criteria to evaluate the reliability of an inverse heat transfer methods.
The criteria are reported below:

1. The predicted temperatures and heat fluxes should be accurate if the measured data are of high accuracy;

2. The method should be insensitive to measurement errors;

3. The method should be stable for small time steps or intervals;

4. Temperature measurements from one or more sensors should be permitted;

5. The method should not require continuous first-time derivatives of the surface heat flux. Furthermore, step changes or even more abrupt changes in the surface heat fluxes should be permitted;

6. Knowledge of the precise starting time of the application of the surface heat flux should not be required;

7. The method should not be restricted to any fixed number of observations;

8. Composite materials should be permitted;

9. Temperature-variable properties should be permitted;

10. Contact conductances should not be excluded;

11. The method should be easy to program;

12. The computer cost should be moderate;

13. The user should not have to be highly skilled in mathematics in order to use the method or to adapt it to other geometries;

14. The method should be capable of treating various one-dimensional coordinate systems;

15. The method should permit extension to more than one heating surface;

16. The method should have a statistical basis and permit various statistical assumptions for the measurement errors;

Appendix C

Description of the Code

Several thousands of lines of code in MatLab have been developed in order to implement the readings of data from IR images and the inverse heat transfer method described in this thesis. A very brief description of the capabilities of the code is given in this appendix.

The method to generate the time depending temperature is the MATLAB tool *pdepe*. It solves initial-boundary value problems for systems of parabolic and elliptic PDEs in the one space variable x and time t. The system coefficient (corresponding to the thermo-physical properties) may be set depending on the system variable (in the case of this work it is temperature). In particular *pdepe* solves PDEs, in case of source term identically equal to 0, of the form:

$$c\left(x, t, u, \frac{\partial u}{\partial x}\right)\frac{\partial u}{\partial x} = x^{-m}\frac{\partial}{\partial x}\left(x^m f\left(x, t, u, \frac{\partial u}{\partial x}\right)\right) \quad \text{(C.1)}$$

The PDEs hold for $t_o \leq t \leq t_f$ and $a \leq x \leq b$. The interval $[a, b]$ must be finite. m can be 0, 1, or 2, corresponding to slab, cylindrical, or spherical symmetry, respectively.

In the eq. C.1 $f\left(x, t, u, \frac{\partial u}{\partial x}\right)$ is the flux term it may be depend on the variable u (that in the present case is the temperature). The coupling of the partial derivatives with respect to time is restricted to multiplication by a diagonal matrix $c\left(x, t, u, \frac{\partial u}{\partial x}\right)$.

Furthermore for $t = t_o$ and all x, the solution components satisfy initial conditions of the form:

$$u\left(x, t_o\right) = u_o\left(x\right) \quad \text{(C.2)}$$

For all t and either $x = a$ or $x = b$, the solution components satisfy a boundary condition of the form:

$$p\left(x, t, u\right) + q\left(x, t\right)f\left(x, t, u, \frac{\partial u}{\partial x}\right) = 0 \quad \text{(C.3)}$$

Elements of q are either identically zero or never zero. Note that the boundary conditions are expressed in terms of the flux f rather than $\partial u/\partial x$. Also, of the two coefficients, only p can depend on u.

The optimizations routine is based on *"lsqnonlin"* MAT-LAB tool that solves nonlinear least-squares (nonlinear data-fitting) problems. It may work according to two different methods: the *trust-region-reflective algorithm* or levenberg-marquardt algorithm. The routine developed in this work uses the former one. This algorithm is a *subspace trust-region method* and is based on the *interior-reflective Newton* method described in Coleman & Li (1994). Each iteration involves the approximate solution of a large linear system using the method of preconditioned conjugate gradients (PCG).

The program gives in output temperature history, all the parameters object of optimization, calculation time and values of correlation between measure and estimated temperature rises. The program is also *user friendly* in the sense that all parameters of interest can be set through clear graphical interface; for example the ambient temperature or emissivity function can be easily input in the code.
Finally, it is possible to use the program just to quickly generate temperature rises with given parameters, to have an idea of how the modification of a certain parameter influences the temperature evolution.

Bibliography

Astarita, T. & Carlomagno, G. M. (2013), *Infrared Thermography for Thermo-Fluid-Dynamics*, Springer.

Aydin, M. (97), 'Dependence of the natural convection over a vertical flat plate in the presence of the ribs', *Int. Comm. Heat Mass Transfer* **24**, 521 – 531.

Aydin, O. & Guessous, L. (2001), 'Fundamental correlations for laminar and turbulent free convection from a uniformly heated vertical plate', *International Journal of Heat and Mass Trasnfer* **44**, 4605 – 4611.

Banks, H. & Kunisch, K. (1989), *Estimation Techniques for Distributed Parameter Systems*, Birkhauser Boston, Boston.

Beck, J. (1985), *Inverse Heat Conduction. Ill-posed Problems*, Wiley-Interscience.

Bertero, M. & Bioccacci, P. (1998), 'Introduction to inverse problems in imaging', *IOP Publishing* . Bristol, UK.

Bhavnani, S. & Bergles, A. (1990), 'Effect of surface geometry and orientation on laminar natural convection heat trasnfer from a vertical plate with transferse roughness elements', *International Journal of Heat and Mass Transfer* **33**(5), 965 – 981.

Cairnie, L. & Harrison, A. (1982), 'Natural convection adjacent to a vertical isothermal hot plate with a high surface-to-ambient temperature difference', *International Journal of Heat and Mass Transfer* **25**(7), 925 – 934.

Cardone, G., Ianiro, A., dello Ioio, G. & Passaro, A. (2012), 'Temperature maps measurements on 3d surfaces with infrared thermography', *Experiments in Fluids* **52**, 375 – 385.

Carter, C. & Norton, M. (2007), *Ceramic Material - Science and Enginering*, Springer. 716.

Chang, C. & Lee, Z. (2008), 'Free convection on a vertical plate with uniform and constant heat flux in a thermally stratified micropolar fluid', *Mechanics Reasearch Communication* **35**, 421 – 427.

Chen, C. & Eichorn, R. (1976), 'Natural convection from a vertical surface to a thermally stratified fluid', *Journal of Heat Transfer* pp. 917 – 923.

Coleman, T. & Li, Y. (1994), 'On the convergence of the interior-reflective newton methods for nonlinear min-

imization subject to bounds', *Mathematical Programming* (67), 189 – 221.

Engl, H., Hanke, M. & Neubauer, A. (1996), *Regularization of Inverse Problems*, Kluwer, Dordrecht.

Franca, F., Ezekoye, O. & Howell, J. (2001), 'Inverse boundary design combining radiation and convection heat transfer', *ASME Journal of Heat Transfer* **123**, 884 – 891.

Gebbie, H. A., Harding, W., Hilsum, C., Pryce, A. & V., R. (1951), Atmospheric transmission in the 1 to 14 micron region, *in* 'Proceedings Royal Society', Vol. 206, pp. 87–107.

Gebhart, B. (1973), 'Natural convection flows and stability', *Advances in Heat Transfer* **9**, 273 – 348.

Green-Spikesley, E. (1979), 'Investment casting', *Material in Enginneering Application* (1), 328 – 334.

Hadamard, J. (1923), *Lecteratures on Cauchy's Problem in Linear Differential Equation*, Yale University Press.

Havet, M. & Blay, D. (1999), 'Natural convection over a non-iso-thermal vertical plate', *International Journal of Heat and Mass Transfer* **42**, 3103 – 3112.

Höhne, G., Hemminger, W. & Flammershein, H. (2010), *Differential Scanning Calorimetry*, second edition edn, Springer.

Hollis, B. (1995), User's manual for the one-dimensional hypersonic experimental aero-thermodynamic (1dheat) data reduction code, Technical Report 4691, NASA Contractor Report, North Carolina State University - Raleigh, North Carolina.

Jones, S., Jolly, M. R. & Lewis, K. (2002), 'Development of techniques for predicting ceramic shell properties for investment casting', *British Ceramic Transaction* **101**(3).

Kingery, W., Bowen, H. & Uhlmann, D. (1976), *Introduction to Ceramics*, 2nd edition edn, Wiley.

Kirsch, A. (1996), *An Introduction to the Mathematical Theory of Inverse Problems*, Springer-Verlag.

Levenberg, K. (1944), 'A method for the solution of certain problems in least squares', *Quarterly of Applied Mathematics* **2**, 164 – 168.

Lin, S. (1978), 'Transient heat conduction with temperature-dependent thermal conductivity by the orthogonal collocation method', *Heat and Mass Transfer* **5**, 29 – 39.

Marquardt, D. (1963), 'An algorithm for least-squares estimation of nonlinear parameters', *SIAM Journal of Applied Mathematics* .

Martynenko, O., Berezovsky, A. & Sokovishin, Y. (1984), 'Laminar free convection from a vertical plate', *Inter-*

nation Journal Heat and Mass Transfer **27**(6), 869 –
881.

Mastrullo, R., Mazzei, P., Naso, V. & R., V. (1991), *Fon-
damenti di Trasmissione del Calore*, Liguori, Naples.

Meola, C., Carlomagno, G., Squillace, S. & G., G.
(2002), 'Non-destructive control of industrial materials
by means of lock-in thermography', *Meas. Sci. Technol.*
13, 1583 – 1590.

Merritt, T. P. & Hall, F. F. (1959), Blackbody radiation,
in 'Proceeedings of the IRE', Institute of Radio Engi-
neering.

Mishra, S., Talukdar, P., Trimis, D. & Durs, F. (2005),
'Two-dimensional transient conduction and radiation
heat transfer with temperature dependent thermal con-
ductivity', *International Communications in Heat and
Mass Transfer* (32), 305 – 314.

Mitchell, A. (1999), *Investment Casting*, New Castings
Direction for Gas Turbine Construction.

Modest, M. (2003), *Radiative Heat Transfer*, second edi-
tion edn, Academic Press.

Moré, J. & Sorensen, D. (1983), 'Computing a trust re-
gion step', *SIAM Journal on Scientific and Statistical
Computing* **3**, 553 – 572.

Morozov, A. (1993), *Regularization Methods for Ill-Posed
Problems*, CRC Press, Boca Raton, FL.

Mustafa, E. (2001), 'Fluorophlogopite porcelain based on talcfeldspar mixture', *Ceramic International* **27**(1), 914.

Natterer, F. (1986), *The Mathematics of Computerized Tomograph*, Wiley, New York.

Ostrach, S. (1953), An analysis of laminar free-convection flow and heat transfer about a flat plate parallel to the direction of the generating body force, Technical Report 1111, NACA.

Park, H. & Lee, W. (2002), 'The solution of inverse radiation problems using an efficient computational technique', *Journal of Quantitative Spectroscopy and Radiative Transfer* **73**, 41 – 54.

Parker, W., Jenkins, R., Butter, C. P., Gutter, G. L. & L., A. G. (1961), 'Application physics', *Journal of Application Physics* (32), 1679.

Randall, M. G. (1996), *Sintering Theory and Practice*, Wiley-VCH.

Schmidt, E. & Eckert, E. (1935), 'über die richtungsverteilung der wärmestrahlung von oberflächen', *Forschung im Ingenieurwesen* **6**(4), 175 – 183.

Sidhu, B. S., Kumar, P. & Mishra, B. (2008), 'Effect of slurry composition on plate weight in ceramic shell investment casting', *Journal of Materials Engineering and Performance* **17**(4), 489.

Sparrow, E. & Gregg, J. (1956), 'Laminar free convection from a vertical plate with uniform surface heat flux', *Trans. ASME* **78**, 435 – 440.

Su, G., Tan, Z. & Su, J. (2009), 'Improved lumped models for transient heat conduction in a slab with temperature-dependent thermal conductivity', *Applied Mathematical Modelling* (33), 274 – 283.

Taylor, P. (1983), An illustrated history of lost wax casting, *in* 'Proc. 17th Ann. BICTA Conf.', British Investment Casting Association.

Taylor, R. E. & Maglic, K. (1984), 'Compendium of thermophysical property measurement methods', *Survey of Measurement Techniques* **1**.

Tikhonov, A. N. (1977), *Solutions of Ill-Posed Problems*, Wiley, New York.

Tikhonov, A. N., Leonov, A. S. & Yagola, A. G. (1998), *Nonlinear Ill-Posed Problems*, Vol. I - II, Chapman and Hall.

Touloukian, Y. (1967), *Thermophysical Properties of High Temperature Solid Material*, Vol. 4, McMillman Company.

Tsuji, T., Tsuyoshi, K. & Tatsuhiko, N. (2007), 'Heat transfer enhancement in a turbulent natural convection boundary layer along a vertical flat plate', *International Journal of Heat and Fluid Flow* **28**, 1472 – 1483.

Vogel, C. (2002), *Computational methods for inverse problems*, Frontiers in Applied Mathematics, SIAM.

Yamane, T., Katayama, S. & Todoki, M. (1997), 'Experimental investigation of nonuniform heating and heat loss from a specimen for the measurement of thermal diffusivity by the laser pulse heating method', *International Journal of Thermophysics* **18**.

Yuan, C. & Jones, S. (2003), 'Investigation of fibre modified ceramic moulds for investment casting', *Journal of the European Ceramic Society* (23), 399 – 407.

Acknowledgement